Daedalus: A Low-Flying Spacecraft for the Exploration of the Lower Thermosphere - Ionosphere

Theodoros E. Sarris[1], Elsayed R. Talaat[2], Minna Palmroth[3], Iannis Dandouras[4], Errico Armandillo[5],
5 Guram Kervalishvili[6], Stephan Buchert[7], David Malaspina[8], Allison Jaynes[9], Nikolaos Paschalidis[10],
John Sample[11], Jasper Halekas[9], Stylianos Tourgaidis[1], Vaios Lappas[12], Mark Clilverd[13], Qian Wu[14],
Ingmar Sandberg[15], Anita Aikio[16], Panagiotis Pirnaris[1]

[1] Department of Electrical and Computer Engineering, Democritus University of Thrace, Xanthi, 67132, Greece
10 [2] National Oceanic and Atmospheric Administration, Silver Spring, MD, 20910, USA
[3] University of Helsinki, Helsinki, 00014, Finland
[4] IRAP, Université de Toulouse / CNRS / UPS / CNES, Toulouse, 31028, France
[5] Formerly at ESA/ESTEC, Noordwijk; now Space Engineering Consultant, The Netherlands
[6] GFZ German Research Centre for Geosciences, Potsdam, 14473, Germany
15 [7] Swedish Institute of Space Physics, Uppsala, 75121, Sweden
[8] Laboratory for Atmospheric and Space Physics, University of Colorado, Boulder, CO, 80303, USA
[9] University of Iowa, Iowa City, IA, 52242-1479, USA
[10] NASA Goddard Space Flight Center, Greenbelt, MD, 20771, USA
[11] Montana State University, Bozeman, MT, 59717-2220, USA
20 [12] Athena Research & Innovation Centre, Amarousio Athens, 15125, Greece
[13] British Antarctic Survey, Cambridge, CB30ET, UK
[14] High Altitude Observatory, NCAR, Boulder, CO, 80307-3000, USA
[15] Space Applications & Research Consultancy (SPARC), Athens, 10677, Greece
[16] University of Oulu, Ionospheric Physics Unit, Oulu, 90014, Finland

Correspondence to: Theodore E. Sarris (tsarris@ee.duth.gr)

Abstract. The Daedalus mission has been proposed to the European Space Agency (ESA) in response to the call for ideas for the Earth Observation programme's 10th Earth Explorer. It was selected in 2018 as one of three candidates for a Phase-0 feasibility study. The goal of the mission is to quantify the key electrodynamic processes that determine the structure and
30 composition of the upper atmosphere, the gateway between the Earth's atmosphere and space. An innovative preliminary mission design allows Daedalus to access electrodynamics processes down to altitudes of 150 km and below. Daedalus will perform in-situ measurements of plasma density and temperature, ion drift, neutral density and wind, ion and neutral composition, electric and magnetic fields and precipitating particles. These measurements will unambiguously quantify the amount of energy deposited in the upper atmosphere during active and quiet geomagnetic times via Joule heating and
35 energetic particle precipitation, estimates of which currently vary by orders of magnitude between models. An innovation of the Daedalus preliminary mission concept is that it includes the release of sub-satellites at low altitudes: combined with the main spacecraft, these sub-satellites will provide multi-point measurements throughout the Lower Thermosphere-Ionosphere

region, down to altitudes below 120 km, in the heart of the most under-explored region in the Earth's atmosphere. This paper describes Daedalus as originally proposed to ESA.

1 Introduction

1.1 Science Context

5   The Earth's upper atmosphere, which includes the Lower Thermosphere and Ionosphere (LTI), is a complex dynamical system, responsive to forcing from above and below: From above, solar radiation, solar wind and solar disturbances such as flares, solar energetic particles and coronal mass ejections cause strong forcing through many complex processes and produce ionization enhancements, electric fields, current systems, heating, and ion-neutral chemical changes, which are not well quantified. From below, the LTI system is affected by atmospheric gravity waves, planetary waves and tides that
10 propagate through and dissipate in this region, with effects that are poorly understood. The response of the upper atmosphere to global warming and its role in the Earth's energy balance is also not well-known: whereas the increase in CO_2 is expected to result in a global rise in surface temperatures, model simulations predict that the thermosphere may cool instead (Rishbeth and Roble, 1992), leading to thermal shrinking of the upper atmosphere; however there is disagreement about the exact cooling trends (Qian et al., 2011; Laštovička, 2013). Quantifying the resulting secular variation in lower thermospheric
15 density is needed for understanding the interplay of solar and atmospheric variability, and it will be critical in the near future, as increased levels of orbital debris cause increased hazards for space navigation, since lower density leads to a slower rate of removal of objects in Low Earth Orbit (LEO) (Solomon et al., 2015). Measurements in the thermosphere are also essential for understanding the exosphere and modelling its altitude density profile and its response to space weather events (Zoennchen et al. 2017), as all exospheric models use parameters from this region as boundary conditions. During
20 geomagnetic storms and substorms, currents with increased amplitudes close through the LTI, producing enhanced Joule heating (Palmroth et al., 2005; Aikio et al., 2012) and leading to significant enhancements in neutral density at high altitudes, which results in enhanced satellite drag. Geomagnetic storms also enhance ionospheric scintillation of the Global Navigation Satellite System (GNSS) signals, which severely degrades positional accuracy and affects the performance of radio communications and navigation systems (Xiong et al., 2016). Sudden enhancements in the current system that closes within
25 the LTI induce currents on the ground, termed Geomagnetically Induced Currents (GICs); the impact of the largest of GICs on power transformers in electrical power systems has, on occasions, been catastrophic and is now included in many national risk registers as it is considered a threat to technology-based societies, should an extreme solar event occur (Pulkkinen et al., 2017), or even repeated smaller events, which can stress transformers and reduce their operational lifetime (MacManus et al., 2017). Despite its significance, the LTI is the least measured and understood of all atmospheric regions: In particular the
30 altitude range from ~100 to 200 km, where the magnetospheric current systems close and where Joule heating maximizes, is too high for balloon experiments and too low for existing LEO satellites, due to significant atmospheric drag. Furthermore, few spectral features emanate from this region; these have been exploited by recent remote-sensing spacecraft and from

ground instrumentation, but despite these advances, this region remains under-sampled with many open questions. For example, no data set is currently available from which the LTI energy budget can be confidently derived on a global basis. Thus it is not surprising that scientists often informally refer to this region as the "ignorosphere". The ever-increasing presence of mankind in space and the importance of the behaviour of this region to multiple issues related to aerospace

5   technology, such as orbital calculations, vehicle re-entry, space debris lifetime etc., together with its importance in global energy balance processes and in the production of GICs and GNSS scintillation make its study a pressing need.

1.2 Initial Mission Concept Overview

The target of the proposed Daedalus mission is to explore the lower thermosphere-ionosphere by performing in-situ measurements of ion, electron and neutral temperature and density, ion drift, neutral wind, ion and neutral compositions,

10   electric and magnetic fields, and precipitating particles. Daedalus is composed of a primary instrumented satellite in a highly elliptical, dipping polar orbit, with a perigee of 150 km, a threshold apogee above 2000 km and goal apogee above 3000 km to ensure a sufficiently long mission lifetime, a high-inclination angle ($>85^{\circ}$), and a number of deployable sub-satellites in the form of CubeSats; four CubeSat sub-satellites are baselined herein, but alternative mission concepts with larger sub-satellites shall also be discussed in the upcoming Phase-0. The main satellite performs several short (e.g., day-long)

15   excursions down to 120 km (perigee descents) using propulsion, measuring key electrodynamic properties through the heart of the under-sampled region. At selected excursions, the main satellite releases the sub-satellites using the standardized PPOD CubeSat release mechanism. The sub-satellites perform a multi-day to months-long orbit that gradually reduces its perigee altitude due to atmospheric drag, eventually burning up in the mesosphere. During each sub-satellite release, co-temporal measurements by the main satellite at higher altitude and the sub-satellite below offer unique and unprecedented

20   synchronized two-point measurements through the LTI region. This measurement scheme allows the investigation of cause-and-effect at different altitudes and offers the opportunity to measure, for the first time, the spatial extent and temporal evolution of key under-sampled phenomena in the LTI. An example of the orbits of the main Daedalus satellite and a deployed sub-satellite are shown in **Fig. 1**.

This paper describes the original Daedalus mission concept as proposed to ESA in response to a call for ideas for the 10th

25   Earth Explorer mission. The proposed concept has evolved from previous work carried out in the context of an ESA-GSTP (General Support Technology Program) study that was performed as part of the Greek Task Force in 2009 (Sarris et al., 2010), with a different set of constraints and accessible spacecraft and measurement technology. Upcoming Phase-0 activities have been put in place to review and consolidate concept, design and requirements within the new set of boundary conditions associated with the Earth Explorer programme.

30   ### 1.3 Measurement Gaps in the LTI

The lowest in-situ scientific measurements performed in this region by orbiting vehicles were made by the Atmosphere Explorer (AE) series of satellites in the 1970's. The perigee of these satellites extended as low as 140 km, but the dynamic

range of some of the key measurements, such as mass spectrometer composition, made the data interpretation difficult at low altitudes. Since then, in-situ measurements in the LTI have been limited to short crossings by sounding rockets, which by nature give only a snapshot of the LTI over a single location, whereas, for example, to understand the spatial structure and temporal evolution of key processes in response to a multi-hour solar storm, longer-term observations are required, across

5   different locations. Density measurements as low as 130 km have been inferred from the decay of low-altitude surveillance satellites, and have been useful for understanding the gross features of the lower thermosphere, but the electrodynamics and composition of the transition region between 100 and 200 km remain obscure. At higher altitudes, a series of spacecraft have provided measurements of electric fields and density (CHAMP, DEMETER, GRACE, C/NOFS), but these are far from the transition region, which remains under-sampled. Thus, information on this region arrives almost exclusively from remote

10   sensing, either from satellites (SME, UARS, CRISTA, SNOE, TIMED, ENVISAT, AIM) or from various ground experiments (Lidars, Ionosondes, Incoherent Scatter Radars, Coherent Scatter Radars, Auroral Imagers, Photometers and Fabry-Perot Interferometers). There is a wealth of information that these measurements are providing, and there are significant advances in LTI science that have been accomplished, but there are also limitations that arise from the nature of remote sensing techniques. For example, density and temperature measurements are unfortunately not possible or are largely

15   inaccurate in the 100-200 km region, as radiances become too weak and non-thermal above that altitude. Some major species composition information is obtained by a combination of UV, IR and FPI measurements, but there is a significant gap in the obtainable profiles at ~100-200 km due to lack of appropriate emissions for observation. It is also noted that different observation methods may produce large deviations (even orders of magnitude) in estimates of key parameters in the LTI, such as conductivity, ion drifts and neutral winds, with no baseline dataset for comparison.

20   **2 Daedalus Science Objectives**

The main scientific objectives are two-fold: On one hand, Daedalus will quantify, for the first time, the key unknown heating processes in the LTI, and in particular the largely unknown Joule heating as well as energetic particle precipitation heating, investigating how these affect the dynamics and thermal structure of the LTI, and how density, composition and temperature of the LTI vary during periods of enhanced heating associated with extreme space weather events. On the other hand,

25   Daedalus will investigate the temperature and composition structure of the LTI in order to address a number of open questions, such as: the processes that control momentum and energy transport and distribution in one of the most unknown regions, the transition region at 100-200 km; the relative importance of the equatorial dynamo in driving the low latitude ionosphere; the coupling of ions and neutrals in the low altitude ionosphere and thermosphere; the role of the LTI region as a boundary condition to the exosphere above and stratosphere below; and the effects of the LTI region in the dynamics of the

30   exosphere and stratosphere. These are discussed in further detail below.

2.1 Heating processes and Energy balance in the LTI

An overview of the energy and transport processes in the LTI resulting from the interaction with the near Earth space can be seen in **Fig. 2**, showing the complexity of simultaneous processes such as: incoming energy from solar and magnetospheric processes; lower atmosphere driving the low latitude ionosphere; Joule heating at higher latitudes; Energetic Particle
5 Precipitation (EPP) along field lines at high latitudes; the Auroral Electrojet - the large (~1 million Amperes) horizontal currents that flow in the E-region (90-150 km) in the auroral ionosphere; and the Equatorial Electrojet - the large eastward flow of electrical current in the ionosphere that occurs near noon within 5° of the magnetic equator. Radiative heating of the LTI by extreme ultra-violet light (XUV) and x-rays from the Sun varies strongly with the 11-years solar cycle and is responsible for the large temperature increase above the mesopause at about 100 km altitude. It's energy input is well
10 measured, however, after subtracting the solar cycle variations, a long term cooling is predicted through atmospheric general circulation models (Rishbeth and Roble, 1992); this was found to be 10-15 K/decade through radar data over 33 years (Ogawa et al., 2014). This is attributed to anthropogenic greenhouse cooling because of increasing absorption of infrared. Joule heating, auroral particle precipitation and solar deposition of energy maximize in the altitude range 100-200 km. At the same time, the composition between molecular and atomic species varies with the electrodynamic energy input and
15 atmospheric forcing, as well as with particle precipitation. These composition variations in turn modulate significantly the efficiency of radiative heating, in both EUV and infrared. The 100-200 km region also involves large gradients and variability in various parameters such as winds, temperature, density and composition; these parameters show different behaviour between different latitudes. The processes that control momentum and energy transport are strongly tied to the spatial and temporal variations of winds, temperature, density and composition; thus, whereas there is a fairly good physical
20 understanding of energy transport processes, there are few measurements of how the energy is redistributed, hindering the exact quantification of these processes and their accurate modelling. Specifically, there is a lack of measurements of E-region electric fields, ion drifts and ion composition and simultaneous measurements of neutral winds and neutral composition.

Estimates of the range of energy input in the LTI by each of the main heating processes discussed above are presented in
25 **Table 1**. What is evident from this table is that the energy source with the largest variation, which can range from comparatively insignificant levels to the single largest energy input, is Joule heating; second to that in both variation and significance is Energetic Particle Precipitation. Particularly at high latitudes and at times of large solar and geomagnetic activity, the Earth's magnetic field couples the LTI to processes in the magnetosphere and the solar wind, which provide heating that rivals or even exceeds the heating of the radiative component. The quantification and parameterization of these
30 processes is one of the primary science objectives of Daedalus.

2.1.1 Joule Heating

Joule heating, or frictional heating, is caused by collisions between ions and neutrals in the presence of a relative drift between the two (Vasyliūnas and Song, 2005). Ion-neutral friction tends to drive the neutral gas in a similar convection pattern to that of the ions, which with time also generates kinetic energy (Codrescu, 1995; Richmond, 1995). Such drifts are

5   driven by processes in the magnetosphere and involve current systems between space and the ionosphere. These currents, marked in **Fig. 2** as field-aligned currents, were first envisaged by Birkeland more than 100 years ago (Birkeland, 1905): they flow parallel to the magnetic field and they couple electrically the high-latitude ionosphere with near-Earth space. The strength of these currents and their structure depend on solar and geomagnetic activity. In space they are well characterized by a number of missions with multi-point measurement capabilities, such as ESA's four-spacecraft Cluster mission (Amm,

10   2002; Dunlop et al., 2002) and the AMPERE mission, using magnetometer measurements from the Iridium satellites (Anderson et al., 2000). However the closure of these current systems, which occurs within the LTI with a maximum current density within the 100-200 km region, is not well sampled. This leads to large uncertainties in understanding and quantifying Joule heating in this region. Joule heating is the most thermo-dynamically important process dissipating energy from the magnetosphere, and it affects many thermospheric parameters, such as wind, temperature, composition and density, in a very

15   significant way; it is thought that its effects on the upper atmosphere are more significant than energetic and auroral particle precipitation (e.g., Zhang et al., 2005), even though the exact ratio has not been successfully quantified to date. In a major magnetic storm, Rosenqvist et al. (2006) estimated the power input into the magnetosphere to be ~17 GW by extrapolating data from the Cluster mission; about 30% of this power could be dissipated as Joule heating in the ionosphere-thermosphere, as inferred from EISCAT radar measurements and AMIE modelling. However, as discussed below, there are great

20   discrepancies in estimating Joule heating, depending on methodology and measurements used.

One of the big unknown parameters involved in Joule heating, and one of the issues that could be a source of the largest discrepancies in its estimates, involves neutral winds, as Joule heating depends on the difference between ion and neutral velocities in a complex way (Thayer & Semeter, 2004). For example, in the auroral oval the role of winds during active conditions is to increase Joule heating in the morning sector, but to decrease it in the evening sector (Aikio et al., 2012; Cai

25   et al., 2013). Due to a lack of co-located and co-temporal measurements, neutral winds are usually neglected, and currently height-integrated Joule heating is more commonly estimated in one of the following ways: (i) from the product of the electric field and the height-integrated current density, $\mathbf{E} \cdot \mathbf{J}$, (ii) from the product of the height-integrated Pedersen conductivity, Σ_P, and the square of the electric field, $\Sigma_P E^2$, where Σ_P is estimated from models, or (iii) from the Poynting theorem, estimating the field-aligned Poynting flux, in which the magnetic field is obtained through differences between measured and modelled

30   values. An overview of various methods to estimate height-integrated Joule heating is described in Olsson et al. (2004).

Traditionally, data sets that have been used for Joule heating estimates include measurements from ground radars (Ahn et al., 1983; Aikio et al., 2012) and from low-altitude satellites, such as AE-C (Foster et al., 1983), DE-1 and DE-2 (Gary et al., 1994) and Astrid-2/EMMA (Olson et al., 2004). Of these measurements DE-1 and DE-2 were the only spacecraft that

performed simultaneous neutral wind and electric field measurements; however they only went down to 567.6 km and 309 km respectively, and, even though the region that the DE spacecraft sampled is certainly heated up after the deposition of energy in the E-region, it is well above the region where Joule heating maximizes. Estimates have also been based on empirical models such as the AMIE assimilative procedure (Chun et al., 1999), the GUMICS-4 MHD model (Palmroth et al.,

5   2004, 2005) and the CEJH empirical model (Zhang et al., 2005).

The uncertainty in obtaining accurate Joule heating estimates between the various methods is evident in **Fig. 3**, by Palmroth et al. (2005), in which Joule heating is calculated through three different ways that are commonly used: on the top plot measurements from the SuperDARN ionospheric radar network are used combined with Polar satellite measurements; on the middle plot it is estimated through parameterizations that are used commonly, using empirical relationships with the AE and

10   Kp indexes as proxies; and on the lower plot by using the AMIE assimilation model from NCAR. What is particularly striking in this plot is that there is up to a 500% difference among some of these estimates. Furthermore, it can be seen that there is a significant difference on the timing (time scale is in hours) of when Joule heating starts: there is almost an hour difference in the onset and peak of Joule heating. This is due to the lack of in-situ measurements where Joule heating occurs and is an issue that is wide open to date. It is therefore of critical importance to fully understand the basic properties of Joule

15   heating and to fully quantify and parameterise its effects, in order to understand the processes in the high latitude ionosphere and thermosphere. The correct quantification of Joule heating is also essential in order to properly and accurately include it in models, thus being able to predict its relation to LTI dynamics and its contribution to the total energy balance. Some questions related to Joule heating that remain open are: **[1]** What is the dependence of Joule heating on geomagnetic activity and on energetic particle precipitation? **[2]** What is the relation of Joule heating to neutral wind, composition, temperature

20   and density? **[3]** What is the Joule heating distribution in space and time? **[4]** What is the time constant for momentum transfer during Joule heating processes, and what is the dependence of this time constant on magnetospheric conditions and thermosphere state? **[5]** What is the relation between Joule heating, upwelling and changes in neutral composition? **[6]** How is Joule heating affecting and/or driving neutral winds at low latitude, what is its impact in redistributing heat, momentum and composition, and how do these changes affect the lower atmosphere? and **[7]** How much Joule heating is involved in the

25   equatorial and mid-latitude tidal dynamos, in gravity waves and how does it affect the neutral atmosphere dynamics?

Since it is the coupling of ions and neutrals that determines Joule heating, in order to understand in-depth the Joule heating process, and furthermore to perform Joule heating modelling accurately, simultaneous measurements of the ion drifts, neutral winds, plasma and composition down to the E-region is crucial, together with measurements of the electric and magnetic fields, as described in further detail in **Section 3.3** below. These measurements have never been performed in-situ below 300

30   km, in the source region where Joule heating maximizes. There are radars that have made such co-located measurements remotely, but these were localized and provided a weakly constrained estimate of what is happening at 300 km. Daedalus employs a complete suite of measurements that will measure all the needed parameters to calculate Joule heating and the thermosphere response and also differentiate under which conditions different approximations for Joule heating could be valid. In order to quantify and understand the Joule heating process, local measurements at its source in the E-region where

Joule heating maximizes are required. It is for this reason that the causal relationship of Joule heating to the thermosphere dynamics remains to this date unresolved and that estimates vary so greatly.

2.1.2 Energetic Particle Precipitation

Energetic Particle Precipitation (EPP) is the second strongest energy source after Joule heating, both in terms of magnitude and variation. Precipitating electrons, protons and Energetic Neutral Atoms (ENAs) deposit their energy into the atmosphere at different altitudes, depending on particle energy. There are multiple effects caused by EPP: through the collisions with neutral particles at high latitudes, precipitating particles ionize the neutral gas of the lower thermosphere and dissociate atmospheric particles (Sinnhuber et al., 2012); they also heat up the lower thermosphere, produce bremsstrahlung X-rays and auroras and increase the conductivity of the ionosphere. An estimate of the total ionization rate for EPP energies 1, 10 and 100 keV is given in **Fig. 4**. In particular, the increased ionization leads to increased conductivity that facilitates the flow of current along the magnetic field lines and through the ionosphere, thus enhancing Joule heating. However, the direct relationship between EPP and conductivity has not been established. It is therefore important to measure EPP, conductivity and Joule heating at the same time. In addition, EPP (including energies much greater than 100 keV) significantly affects atmospheric composition directly via the production of HO_x and NO_x, and indirectly through the descent of NO_x to lower altitudes (Codrescu et al., 1997; Randal et al., 2007). HO_x and NO_x, act as catalysts for ozone destruction in the mesosphere (e.g., Seppälä et al., 2004), which, through a complicated radiative balance involving the amount of UV, can lead to impact on terrestrial temperatures within the polar vortex (Seppälä et al., 2009). EPP and solar particle forcing on the mesospheric chemistry can be so large that it can affect the atmosphere and climate system (Andersson et al., 2014), and therefore it has received a growing attention also in the Intergovernmental Panel for Climate Change (IPCC) work. The largest issue in relating the mesospheric ozone destruction with magnetospheric processes is that accurate estimations of particle energy spectrum are lacking.

More energetic ions (E>30 MeV) and electrons (E>300 keV) penetrate down to the stratosphere, whereas the "medium" energy ions (1<E<30 MeV) and electrons (30<E<300 keV) deposit their energy through ionization to the mesosphere and the lower energy ions (E<1 MeV) and electrons (E<30 keV) to the thermosphere. ENAs, covering the energy range of ~1 keV to ~1 MeV, are produced via charge exchange when energetic ions interact with background neutral atoms such as Earth's geocorona. Most of the energy density of ENAs is in the ~100 keV range. The energy transfer to the thermosphere due to precipitating ENAs can be significant, particularly during heightened geomagnetic activity. Since they don't follow magnetic field lines these particles play a role in mass and energy transfer to lower latitudes beyond the auroral zone. (Fok et al, 2003). Measurements of EPP have been performed by multiple rockets as well as by various satellites; however, rocket measurements are by nature short in duration, providing essentially only snapshots of vertical profiles, thus failing to capture all phases of EPP and its effects on the LTI. EPP can also be estimated by inverting the electron density height profiles measured by IS radars (e.g. Semeter and Kamalabadi, 2005). The inversion methods are based on ionization rate profiles like those shown in **Fig. 4**, but the profiles depend on thermospheric density and temperature (Fang et al., 2010), which are taken

from models. On the other hand, spacecraft such as POES, DMSP, SAMPEX, Polar and DEMETER have only performed EPP measurements at higher altitudes, failing to measure in-situ the direct effects of EPP on lower thermospheric density, temperature and composition. Several of these missions were also limited by having particle detectors with wide energy channels (POES), whereas others could not resolve pitch angle distribution (DMSP). There is also considerable noise

5 between the electron and ion channels onboard POES SEM-2 instruments, making unambiguous measurements of EPP difficult (Rodger et al., 2010).

In summary, it can be stated that Joule heating and EPP are critical parameters in understanding high-latitude and mid-latitude processes in the LTI. Many aspects of the Joule heating process are not well characterized, and estimates of the energy deposition vary greatly depending on the calculation method. EPP is a critical parameter of high-latitude energy

10 deposition that also affects Joule heating through altering conductivity. The combined measurements of neutral constituents and energetic particles (ions, electrons and neutral atoms) is critical in estimating EPP energy deposition and for better understanding of ionosphere-thermosphere coupling, and will allow scientists to resolve open questions about ion-neutral interaction. Understanding both processes is imperative in understanding atmosphere as a whole.

2.1.3 Science questions related to Heating processes and Energy balance in the LTI

15 Related to the first science objective of Daedalus, key Science Questions that will be addressed by Daedalus are:

- What is the energy that is deposited into the LTI via Joule heating and particle precipitation and how does it affect the dynamics and the thermal structure of the LTI (neutral density and wind, ion and neutral compositions, and temperature)?
- What processes control momentum and energy transport and distribution in the transition region, at 100-200 km

20 altitude range in the high-latitude region?

2.2 Investigation of variations in the temperature and composition structure of the LTI

The second science objective of Daedalus involves the investigation of the temporal and spatial variability of key variables in the LTI system. An overview of this variability can be seen in **Fig. 5**, showing the extreme values of neutral temperature at different solar conditions (left), constituents of the thermosphere (centre) and constituents of the ionosphere (right) as a

25 function of altitude. These are further discussed in the following paragraphs.

2.2.1 Temperature structure of the LTI

In the left panel, it can be seen that the region from ~100-200 km is the transition region where the temperature increases drastically from the mesopause to the thermosphere; higher up (particularly above 300 km) the thermosphere is essentially isothermal. Temperature in the mesosphere (50-85 km) decreases with altitude, reaching a minimum at the mesopause;

30 above that, in the thermosphere temperature increases, and may range from 500 to 2000 K depending on solar and other energy inputs, as well as on energy transport processes. The time-scales of temperature variations within this region also

vary significantly from the lower-end to the upper-end of the transition region: whereas in the mesosphere temperature measurements from ground-based lidars show a diurnal variation, remote sensing measurements of the region above 150 km show a semi-diurnal variation. Many details of these time-scales are not well understood.

2.2.2 Composition structure of the LTI

5 A major characteristic of the neutral composition in the thermosphere is that, contrary to the mesosphere and stratosphere below, its main chemical constituents, N_2, O_2, O, He and H tend to diffusively separate according to their individual scale heights. In particular, the region from ~100 to 200 km, i.e. the region just above the turbopause, is believed to be the key area where this transition takes place: Below a height of ~105 km, turbulence mixes the various species of gas that make up the atmosphere and the relative abundances of species tend to be independent of altitude. This turbulent mixing process is

10 probably related to gravity wave breaking, but it is not known where and how the transition from turbulent mixing to molecular diffusion occurs or how it varies globally, annually or on other time-scales. On the other hand, in the thermosphere above ~200 km, composition is controlled by molecular diffusion; thus heavier species are concentrated lower down, while the light ones dominate at the higher altitudes, so that, to first order, the density of each species decreases with altitude at a rate that is related to its mass, according to $n_x(z) = n_0 e^{-z/H}$, where $H = RT/m_x g$, m_x is the mass of the species in

15 atomic units and R is the gas constant. Due to this diffusive separation, the main species N_2, O_2 and O show variations in their densities that follow the lines of **Fig. 5**, as marked. From this figure, it can be seen that O becomes the dominant species from about 200 km up to the top of the thermosphere. Below 200 km N_2 is the most significant species, whereas below about 120 km O_2 is more significant than O. The most abundant constituent from ~170-200 km and up to ~700 km is O, which plays an important role in the energy balance in the lower thermosphere: O is responsible directly or indirectly for almost all

20 of the radiative cooling of the lower thermosphere by influencing the main radiative cooling terms, CO_2 at 15 μm and NO at 5.3 μm (Gordiets et al., 1982), and thus it affects the response of the LTI to climate change. In particular, regarding NO, despite the great amount of community effort in measurements and modeling, the temporal and spatial variability and magnitude of the concentration of NO observed in the lower thermosphere remains largely unknown. Quantifying the variability of O and O_2 and the sources of this variability is a central challenge in upper atmosphere physics, and will assist

25 in obtaining a better theoretical understanding of upper atmosphere energetics and dynamics.

2.2.3 Science questions related to the temperature and composition structure of the LTI

In summary, temperature and composition structure in the lower thermosphere is extremely important for many processes and remains under-sampled to a large degree, and many details of the time-scales of its variation in the LTI region are not well understood. Related to the second science objective, key science questions that will be addressed by Daedalus are:

30 • What are the spatial and temporal variations in density, composition and temperature of the neutral atmosphere and ionosphere at altitudes of 100-200 km altitude, with respect to solar activity?

- What is the relative importance of the equatorial and mid-latitude tidal dynamos in driving the low and mid latitude ionosphere and how do ions and neutrals couple?

- What is the LTI region's role as a boundary condition to the exosphere above and stratosphere below and how does it affect their energetics and dynamics?

3 Daedalus Mission Requirements

3.1 Orbital Requirements

To resolve the above open questions, there is a need for measurements at different altitudes throughout the LTI and down to extremely low altitudes where key electrodynamics processes such as Joule heating and EPP maximize, for an extended time period. This is best realized by a spacecraft in a highly elliptical orbit, with a perigee that reaches as low as possible in the 100-200 km region; orbital simulations indicate that a nominal perigee of 150 km is feasible for a prolonged mission. In order to perform measurements below the "observation barrier" of 150 km, the spacecraft performs several perigee descents to lower altitudes, down to 120 km by use of propulsion. In order to perform measurements for a duration beyond one year, an apogee higher than 2000 km is required, as discussed below. Most dynamic processes in the LTI, and in particular Joule heating, maximize at high latitudes; thus a high inclination orbit is preferred. Finally, in order to investigate the cause-and-effect of dynamic upper atmosphere processes, and to unambiguously differentiate between spatial and temporal effects, co-temporal measurements at different altitudes are required. This can be achieved by releasing from the main satellite expendable sub-satellites that carry minimal instrumentation and which perform a spiralling orbit until they burn up in the mesosphere. Such multi-point measurements offer the opportunity to measure, for the first time, the spatial extent and temporal evolution of key under-sampled phenomena in the LTI.

3.2 Mission Duration

The LTI is highly variable, being influenced by variations in the solar, auroral, tidal and gravity wave forcing. These variations occur over different time-scales: solar cycle (11-year), inter-annual (e.g., quasi-biennial), seasonal, and most importantly diurnal. While multi-year missions to investigate solar cycle effects may be impractical in the LTI due to high atmospheric drag, it is important to perform measurements in the thermosphere and ionosphere for as much of the diurnal cycle, sampling the same latitude more than once during each season. A high inclination elliptical orbit, such as is required to address key science objectives in the LTI, means that the orbit precesses in latitude over time. In order to provide coverage of all latitudes, and also to sample the LTI region at different seasons, the minimum mission duration is one year, and ideally three years, as a three year mission will significantly enhance measurement statistics of the response of the LTI to solar events at different latitudes and will enhance the observational statistics of seasonal variations in key parameters and processes.

The mission lifetime will depend on a number of parameters, such as apogee selection, spacecraft mass and cross-section, spacecraft drag coefficient and the expected solar activity, which affects atmospheric density and the associated spacecraft drag. In **Fig. 6** we plot the expected Daedalus lifetime in days for different launch dates; the different curves correspond to different spacecraft wet mass at launch (i.e., including propellant mass) and initial spacecraft apogee selection.

5 At the background of **Fig. 6**, the expected solar activity index F10.7 is calculated by Monte Carlo sampling of the six past solar cycles. Lifetime simulations were performed using ESA's DRAMA software, assuming a drag coefficient of 2.2 (suitable for a cylindrical satellite) and a total satellite drag area of 0.6 m^2 (including the electric and magnetic field booms). It is noted that increasing apogee altitude increases the mission lifetime, but leads to enhanced radiation exposure in the inner radiation belt. This should be studied as part of a trade-off analysis, to be conducted during the initial Daedalus mission

10 phases. Finally, it is emphasized that the simulated lifetimes in **Fig. 6** correspond to natural decay times, which can be significantly enhanced with perigee/apogee maintenance by use of propulsion.

3.3 Measurement Requirements

In order to obtain accurate estimates of in-situ Joule heating, which is part of the Daedalus primary mission objective, a number of parameters need to be measured. These are described below, through two commonly accepted expressions for

15 Joule heating estimates. The first one is:

$$Q_J = \boldsymbol{j} \cdot (\boldsymbol{E} + \boldsymbol{u_n} \times \boldsymbol{B}) , \tag{1}$$

where $\boldsymbol{j}$ is the electric current density, $\boldsymbol{E}$ and $\boldsymbol{B}$ the electric and magnetic fields, respectively, and $\boldsymbol{u_n}$ the neutral wind velocity. $\boldsymbol{j}$ can be inferred from magnetometer data, which is, however, not straightforward at altitudes where Pedersen, Hall and Birkeland currents co-exist and all contribute to the local magnetic field, i.e. roughly below 300 km. Alternatively,

20 assuming quasi-neutrality, i.e. that the electron density N_e is equal to the sum of the ion species densities N_{O^+}, $N_{O_2^+}$, and N_{NO^+}, and denoting the electron and ion drifts for each species with $\boldsymbol{v_e}$, $\boldsymbol{v_{O^+}}$, $\boldsymbol{v_{O_2^+}}$, and $\boldsymbol{v_{NO^+}}$, respectively, we can replace $\boldsymbol{j}$ in **Eq. (1)** as per **Eq. (2)**:

$$Q_J = e\big(N_{O^+}\boldsymbol{v_{O^+}} + N_{O_2^+}\boldsymbol{v_{O_2^+}} + N_{NO^+}\boldsymbol{v_{NO^+}} - N_e\boldsymbol{v_e}\big) \approx eN_e(\boldsymbol{v_i} - \boldsymbol{v_e}) \cdot (\boldsymbol{E} + \boldsymbol{u_n} \times \boldsymbol{B}) , \tag{2}$$

For the approximate equality we assume that all ion species drift with the same velocity $\boldsymbol{v_i}$. For strongly magnetized

25 electrons, which is a good assumption throughout the ionosphere down to below 100 km altitude, $\boldsymbol{v_e} \approx \boldsymbol{E} \times \boldsymbol{B}/|B|^2$ is determined by measurement of $\boldsymbol{E}$ and $\boldsymbol{B}$. In-situ measurements of ion drifts, neutral winds, N_e, and of $\boldsymbol{E}$ and $\boldsymbol{B}$ in an arbitrary non-relativistic reference frame (for example the satellite's reference frame) allow the estimate of the total local heating rate. A different method to estimate Joule heating with in-situ measurements, involves Ohm's law applied to ionospheric plasma and estimates of the ion-neutral collision frequencies. Ohm's law for the ionosphere with the electric field in the neutral

30 reference frame $\boldsymbol{E^*} = \boldsymbol{E} + \boldsymbol{u_n} \times \boldsymbol{B}$ is:

$$j_\perp = \sigma_P E^* - \sigma_H E^* \times B/|B|, \tag{3}$$

with σ_P and σ_H the Pedersen and Hall conductivities. Then **Eq. (1)**, assuming no parallel electric field, $E_\parallel = 0$, becomes

$$Q_J = \sigma_P (E^*)^2 = \sigma_P (E + u_n \times B)^2. \tag{4}$$

In **Eg. (4)**, the Pedersen conductivity, σ_P can be calculated as:

5    $$\sigma_P = \frac{q_e}{B}\left[N_{O^+}\frac{r_{O^+}}{1+r_{O^+}^2} + N_{O_2^+}\frac{r_{O_2^+}}{1+r_{O_2^+}^2} + N_{NO^+}\frac{r_{NO^+}}{1+r_{NO^+}^2} + N_e\frac{r_e}{1+r_e^2}\right], \tag{5}$$

In **Eq. (5)**, r_i represents the ratios of each species' collision rate versus its gyrofrequency. The collision rates depend on a number of terms, such as: on the density and composition of the ion and neutral species, which need to be measured independently through mass spectrometry; on the ion and electron temperatures; and on the values for collision cross sections. The latter are calculated primarily through laboratory experiments of ion-neutral collisions. However, these may

10   have systematic uncertainties in the upper atmosphere, and their accuracy has never been evaluated in-situ. These measurements, through the comparison of the two methodologies described above, will also allow a new estimate of collisional cross sections, which are needed and widely used in simulations, analysis of radar data etc.

Daedalus will have a complete suite of instruments to compare the two methodologies and to resolve which approximations are valid. In summary, to evaluate all the parameters that go into Joule heating calculation in a local volume of space, the

15   required measurements are: neutral winds, ion drifts (along track and cross-track), ion density, ion composition and ion temperature, electron temperature, neutral density, neutral composition (primarily N_2, O, O_2, N, NO) and neutral temperature, magnetic field, DC electric fields and DC currents.

In **Fig. 7** simulation results for Joule heating are plotted based on two physics-based models: TIE-GCM (left) vs. GUMICS (right) for the same instance during the storm of April 6th, 2000, and with the same dynamic range for Joule heating (same

20   color-scale). A large discrepancy is seen between the two models, both in total amplitude but also in the spatial features. A spacecraft that performs measurements of the actual parameters that go into Joule heating at various altitudes, and in particular at the region where it maximizes, is the only way to provide an accurate reference for models and to identify missing physics or inaccurately derived parameters.

As a preliminary step towards identifying the observation requirements of Daedalus, a number of upper atmosphere models

25   have been run and inter-compared in order to simulate the measurement performance requirements and dynamic ranges of the proposed instruments. These models, together with the corresponding outputs that are related to Daedalus, are listed below.

- **TIE-GCM:** T_n, T_i, T_e, Zonal, Meridional and Vertical winds, O, O_2, O^+, O_2^+, NO^+
- **GUMICS-4:** Magnetic Field, Electric Field, Pedersen and Hall conductivities, Energetic particle precipitation
30   Energy deposition, Joule heating, Field Aligned Currents
- **IRI-07:** N_e, T_e, T_i, O^+, O_2^+, NO^+

- **NRLMSISE-00:** T_n, O, O_2, Neutral density, Collision frequency
- **FMI - Alpha parameter:** Pedersen to Hall conductivity ratio
- **HWM-07:** Zonal neutral winds, Meridional neutral winds

5   As an example of the sampling of some of the above variables by Daedalus, the simulated storm-time zonal and meridional winds are shown in **Fig. 8**; the simulated ground track of the orbit of a spacecraft that is sampling these winds is also plotted. The dynamic ranges of these variables (i.e., the geophysical quantities to be observed by Daedalus) were estimated by running the above models through extreme (minimum and maximum) geomagnetic activity conditions; in addition, the sensitivity of the variables to model input parameters were investigated. An error analysis was conducted that modelled the

10   sensitivity of the resulting Joule heating to errors in obtaining each of these variables. A summary of the preliminary estimates for the dynamic range in the region of interest and threshold accuracy and sensitivity of proposed key instrumentation is listed in **Table 2** below; these will need to be re-defined through a trade-off analysis as part of the initial phases of the mission development, through an iterative process that involves science goals, instrument specifications, spacecraft capabilities, and mission (orbit) analysis.

15   **3.4 Instrumentation Requirements**

The proposed suite of instruments to perform measurements of the parameters that go into Joule heating and particle precipitation is listed in **Table 2**. The corresponding measured parameters, their dynamic ranges in the region of interest, and the required threshold accuracy and sensitivity for each observable are also listed. Key scientific instrumentation that is placed in the ram direction includes the IDM & RPA or TII, RWS & CWS and the IMS & NMS. The total surface area of

20   the ram direction instrumentation will determine the total cross-section of the spacecraft, which affects the mission lifetime; hence care should be taken during the initial mission phases to minimize the total ram instrument surface. Three-axis stabilization is required for instruments IDM & RPA or TII, RWS & CWS, IMS & NMS, with stringent attitude control and pointing knowledge requirements.

4 Daedalus Mission Concept Overview

25   **4.1 Orbital Design**

Addressing the scientific objectives of Daedalus requires a spacecraft in a high-inclination (>85°) orbit that can perform measurements at high latitudes within the altitude range of 100-200 km for a threshold duration of one year and a goal duration of more than three years, in order to capture the response of the LTI region during all seasons and at all latitudes. Preliminary orbital simulations indicate that this is feasible by a spacecraft with a perigee as low as 150 km and apogee

30   higher than 2000 km. By using an efficient propulsion system the total mission duration can be significantly increased (up to

several years). The need to minimize atmospheric drag is best realized by a torpedo-shaped spacecraft with a minimal cross-section towards the ram direction and with body-mounted solar panels. The mission scenario includes the following parts, shown in the schematic of **Fig. 9**:

- **Part A:** A satellite in a highly elliptical, dipping, high-inclination orbit with a perigee of 150 km and apogee sufficiently high so as to maintain a mission lifetime above a threshold duration of one year and a goal duration of three years performs in-situ measurements down to 150 km.

- **Part B:** The satellite periodically descends to 120 km altitude at selected passes using an efficient propulsion system, performing measurements for a duration of one or more days and subsequently ascends to the nominal perigee altitude of 150 km. At lowest perigee altitude the main satellite releases expendable sub-satellites.

- **Part C:** The sub-satellites are equipped with instrumentation such as a combination of accelerometers, magnetometers and ion-neutral mass spectrometers, and complement the main satellite measurements at low altitudes, providing critical 2-point estimates that enable the determination of the spatial extent and temporal evolution of key electrodynamics processes below 120 km.

A simulation of the evolution of perigee and apogee for a sample mission scenario is shown in **Fig. 10**. This scenario includes a perigee of 150 km, apogee of 3000 km, spacecraft dry mass of 300 kg, propellant mass of 100 kg, and 21 perigee descents ("deep-dips") from 150 km to 120 km. This simulation also includes perigee and apogee maintenance by use of propulsion. With red are presented the osculating elements which include the short-term, the long-term and the secular perturbations on the orbit, and with yellow are presented the Brouwer-Lyddane short mean elements i.e. averaging out the short-term perturbations of the orbit according to the Brouwet-Lyddane theory (Brouwer, 1959 and Lyddane, 1963).

4.2 Instrumentation

In the following we provide details and requirements on the instruments that are proposed in order to address the scientific objectives of Daedalus.

4.2.1 Ion Drift Meter (IDM) and Retarding Potential Analyzer (RPA), or Thermal Ion Imager (TII)

Ion drifts are needed to separate neutral wind dynamics from plasma motions in order to study Joule heating in the high latitude LTI and to investigate the E-region and F-region dynamos at low latitudes. For Daedalus, the following options are considered: An Ion Drift Meter (IDM) combined with a Retarding Potential Analyzer (RPA) or a Thermal Ion Imager (TII).

Description of the IDM: For the Ion Drift Meter (IDM), two sensors will be employed to directly derive the ion drift velocity: a Retarding Potential Analyzer (RPA) to measure the plasma energy distribution along the sensor look direction, and a planar Ion Drift Meter (IDM) to measure the arrival angle of the plasma with respect to the RPA sensor look direction. The RPA will obtain ion temperature, drift velocity, and concentration by measuring incident variations in the ion flux. The IDM will be used to obtain the arrival angle of the ions: in a common design, it is divided symmetrically into four equal pie shaped segments, and it has a square aperture with sides parallel to the pie cuts. Therefore, any off-axis flow of ions results

in different currents in the four segments. This permits the transverse components of ion drift velocity to be measured. When the other sensors face along the s/c velocity vector, the measured ion energy spectra can be used to deduce the component of ion drift in that direction. Therefore, together with the RPAs the instrument is able to obtain the complete ion drift vector. The IDM will also control the bias of a plate on the spacecraft's ram side, and will measure the plate current. For constant

5   bias the ion density can be estimated with high time resolution. A sweeping Langmuir mode will allow measurement of the electron temperature as well. IDMs and RPAs have been widely used for studying ionospheric plasmas, obtaining measurements from high altitude sounding rockets (*Fang and Cheng, 2013*), on the Atmosphere Explorers (AE) and the Dynamics Explorers (DE) (*Hanson et al., 1981*), on the Communications/Navigation Outage Forecasting System (C/NOFS) (*Huba et al., 2014*), and on Defense Meteorological Satellite Program (DMSP) satellites (*Fang and Cheng, 2013*).

10   **Description of the TII:** A Thermal Ion Imager (TII) has some heritage from an IDM/RPA, but also considerable differences from the IDM/RPA concept, in that each of the two TII sensors use an electrostatic focusing system to produce two-dimensional (angle-energy) images of low-energy ion distribution functions; ions are directed to a micro-channel plate (MCP), from where the signal is amplified and converted to an optical one with a phosphor screen. A CCD camera records 2D images of the ion distribution. Calculating the 1st and 2nd moments (partially on-board to reduce telemetry requirements)

15   gives the ion drift velocity vector and the ion temperature. For a full 3D distribution two TIIs oriented in orthogonal planes are needed (with redundant measurements in the direction of the s/c velocity). All particles entering the instrument contribute to observed images giving theoretically high sensitivity and good time resolution. TIIs are a relatively new development (e.g., Knudsen et al., 2003) and have been flown on suborbital sounding rockets, on the Canadian ePOP satellite (a version for electrons), and on the ESA Swarm satellites. On Swarm 1st moments of 2D images can be obtained at 16 Hz

20   corresponding to about 500 m spatial resolution. Full 3D ion velocity vectors and (potentially anisotropic) temperatures are provided at 2 Hz (~3.5 km). As the s/c electric potential affects significantly the measurements, the Swarm TIIs are complemented with Langmuir Probes, which also provide the plasma density eliminating the need for a highly accurate calibration of the total TII particle fluxes. Some of the scientific results that have come from past TII measurements include the characterization of mechanisms responsible for highly localized ion heating cavities (Burchill et al., 2004; Knudsen et al.,

25   2004), observations of ion upflow at speeds of hundreds of m/s within the polar cusp/cleft (Burchill et al., 2010), and precision measurements of ion demagnetization versus altitude in the collisional lower ionosphere (Sangalli et al., 2009; Burchill et al., 2012). Sangalli et al. (2009) compared TII-measured ion drifts with double-probe electric field and neutral velocity measurements to establish a measurement accuracy of better than 20 m/s root-mean-square (RMS).

  IDM/RPAs have often been used to also infer the electric field from the ion drifts, assuming that the ambient plasma is

30   strictly subject to an ExB drift; also on Swarm the EFI (electric field instrument) is actually a TII/LP ion drift combo without any direct electric (E) field measurement. Similarly, if the electric fields are measured using a double-probe electric field instrument, then the ion drifts can be calculated under the same assumption. However that is an assumption that cannot be made safely much below 200 km, as at about 150 km the ion gyrofrequency drops below the ion collision frequency (see,

e.g., Kivelson and Russell 1995, Fig. 7.8). For this reason, both an electric field instrument and an ion drift meter are required.

An IDM or TII for Daedalus will need to be able to handle a mixture of molecular ions (N_2^+, O_2^+, NO^+) and atomic oxygen (O^+), at least at lower altitudes below ~300 km. These are expected to have different ion drifts v_i and, because of the mass difference, of the composition of molecules and O^+, and of the ion temperature T_i dependence, could not be derived independently in RPA sweeps, or could be detected in a TII image at different locations for the same drift/temperature. Instruments on previous missions sometimes separated O^+ from H^+ and He^+, which is easier because of different masses by a factor of >=4. The mass ratio of molecular ions and O^+ is ≈<2. The transition between a plasma dominated by molecular ions and one by O^+ occurs between roughly 150 and 250 km altitude. Also Incoherent Scatter Radars (ISRs) have problems to distinguish between molecular ions and O^+ because of noise in the signals and also because of the relatively small mass difference. A fallback solution is to use a relative composition from a model and fit T_i (ISR) or T_i and v_i (in-situ ion instrument). It should be noted, however, that models like the IRI-07 do not always give an accurate composition.

4.2.2 Ram Wind Sensor (RWS) and Cross-Track Wind Sensor (CWS)

Studies of the kinetics of neutral particle flow in the free molecular flow regime of the satellite environment led early on to various concepts for neutral wind measurements. Based on these concepts, measurements have since resulted in a large body of data of high spatial resolution. These data have revealed an unexpectedly complex and variable neutral atmosphere, a signature of the deposition of large and highly variable quantities of energy. To resolve neutral winds two sensors will be used on Daedalus: a Ram Wind Sensor (RWS) and a Cross-track Wind Sensor (CWS).

Description of the RWS: The Ram Wind Sensor (RWS) will obtain the neutral wind speed along the ram direction of Daedalus by performing a retarding potential energy analysis on an ionized fraction of the flowing neutral gas. In such configuration the incident ambient ions are electrostatically deflected from the instrument axis so that only the ions produced from the flowing neutral beam have access to the electron multiplier detector.

Description of the CWS: The Cross-track Wind Sensor (CWS) will obtain the cross-track neutral wind velocity by measuring small pressure differences created by the bulk motions of the thermal neutral gas in directions perpendicular to the motion of the satellite. In the design employed by the CINDI instrument on-board C/NOFS (Earle et al., 2007, 2013), the neutral wind instrument included four apertures on a hemispherical cover and operated by measuring the arrival angle of the neutral wind at the satellite by detecting small pressure differences between neighbouring chambers with orifices pointing in different directions (Hanson et al., 1992). The pressure measured in four cavities behind these apertures was related to the arrival angle of the neutral gas relative to each aperture normal. Combined with detailed knowledge of the spacecraft velocity vector, the pressure differentials between diametrically opposed cavities allowed the cross-track wind speed to be determined in the satellite frame of reference. Ion gauges in each chamber measured currents proportional to the pressure and ionization efficiency of any given neutral species (O'Hanlon, 1989). Both the CWS and the RWS will face in the ram direction. It is noted that uncertainties in the wind velocity measurements can be introduced by small alignment errors during

instrument installation on the satellite, as through pointing errors in satellite attitude control or determination. A second source of error can be introduced due to noise in the instrument electronics; these errors can influence both absolute and relative measurements of velocities in the medium.

4.2.3 Accelerometer (ACC)

5 The accelerometer on-board Daedalus will measure non-gravitational accelerations such as air drag, Earth albedo and solar radiation acting on the satellite. The direct measurement of acceleration α due to air drag can in turn be used to derive the total atmospheric mass density ρ, through the fundamental relationship: $\alpha = \frac{1}{2}\,\rho\,V^2\,C_d A\,/\,m$, where C_d, A, m, and V are the s/c coefficient of drag, cross sectional area, mass, and velocity respectively (Hedin, 1991). Accelerometer data can also be used to derive winds in the thermosphere (Sutton et al., 2007; Doornbos et al., 2010; Dhadly et al., 2018). Using expected

10 values of these parameters and obtaining values for ρ from the NRLMSISE-00 atmosphere model, it is calculated that the drag acceleration will be on the order of 10^{-7}g at 500 km and 10^{-3}g at 120 km. This level of dynamic range is easily accomplished with 16-bit analog-to-digital conversion. In order to obtain spatial resolution of ~1 km, a sampling frequency of 16 Hz is required for a typical s/c velocity of ~8 km/s. Spatial resolution on the order of ~1 km is sufficient for resolving Joule heating on a scale that can be compared to current models as well as for the detection of gravity waves in the lower

15 thermosphere. Sensitivity of ~10^{-7}g will also allow the measurement of wind velocities around perigee. Acceptable measurement errors are ±10% at 500 km and ±2% at altitudes below 200 km. In addition there may be a systematic error of up to ±3% due to drag coefficient uncertainty. The accelerometer measurements will also monitor the thrust of the propulsion system: a sensitivity on the order of ~10^{-4}g to 10^{-3}g is sufficient to accurately capture the orbit adjustments and deep-dips of the spacecraft. A typical high-precision accelerometer configuration consists of three single-axis

20 accelerometers, mounted mutually at right angles and the instrument determines the applied acceleration from the electrostatic force required to re-center a proof mass. The output is a digital pulse rate proportional to the applied acceleration.

It is noted that the combination of an Accelerometer and reaction wheels of the Attitude and Orbit Control Subsystem (AOCS) of the satellite will introduce restrictions on the usability of the accelerometer, at least for parts of the orbit. As part

25 of the early phases of Daedalus development, these will be further explored. Alternatively, it will also be investigated whether the Mass Spectrometer of the satellite can be used to derive density with sufficient accuracy for the mission needs.

4.2.4 Energetic Particle Detector Suite (EPDS)

The Daedalus EPDS will consist of three distinct instruments: a High Energy Instrument (**HEI**), a Low Energy Instrument (**LEI**) and an Energetic Neutral Atom (**ENA**) instrument. All three will be mounted to the spacecraft with a clear upward-

30 looking Field-of-View (FoV) that will allow full pitch angle (pa) coverage of precipitating particles.

HEI will provide high-resolution differential energy measurements of relativistic electrons and protons/heavy ions precipitating into the LTI environment, with pitch angle resolution capable of resolving the distributions of EPP flux within

the bounce-loss-cone. Electron measurements will be performed in an energy range spanning <40 keV to >1 MeV and protons/heavy ion measurements from <1 MeV to >10's MeV. HEI will be based on a solid-state detector, combining recent advancements in solid-state detector design. The design will need to include detailed modelling of energetic particle-matter interactions such as GEANT4 simulations, to employ Digital Signal Processing (DSP), and to be able to support advanced

5 real-time characterization algorithms and counting rates up to 10^6 counts/sec. A primary benefit of utilizing DSP is pile up detection and recovery, making dead time essentially negligible after correction.

LEI will consist of an electron sensor and a proton sensor: The LEI electron sensor will provide the 3D velocity distribution (fluxes vs. energy and pitch angle) of thermal and supra-thermal electrons in an energy range spanning <30 eV to >30 keV. The LEI proton sensor will provide energy coverage between >1 MeV, which is the proton threshold of HEI, and the few eV

10 or 10s eV ions measured by the IMS (see following section). It is noted here that precipitating ions of a few 10s keV can lead to significant enhancements of electron density and conductivities (e.g., Yuan et al., 2014). Heritage electron sensors have already performed measurements at the altitudes of Daedalus on a number of rocket flights, and have returned excellent science data. Heritage sensors commonly utilize an electrostatic analyser to provide measurements of precipitating electrons at high cadence with high energy and pitch angle resolution, enabling quantification of the energy input into the

15 thermosphere and ionosphere. Electrostatic analysers are well understood and have high heritage (Doss et al., 2014), dating back to the original Carlson et al. (1983) top-hat design. Electrostatic analysers bias the inner of two concentric hemispheres to a positive voltage to select electrons by energy, with high energy and angular resolution ensured by the natural focal properties of the electrostatic analyser. Electrostatic analysers count individual particles, typically utilizing micro-channel plate (MCP) detectors with a segmented anode to collect charge pulses, and charge-sensitive amplifiers to convert pulses into

20 digital counts. For Daedalus, electrostatic deflectors will be required to increase the FoV to cover at least ~70% of the distribution (Sauvaud et al., 2008), including upward-going and downward-going electrons. Upward-going electrons provide information about magnetic and electric fields below the spacecraft, and are therefore a secondary science topic. Measurements will need to be made fast enough to resolve spatial structures ~100 km, requiring 10 s or better cadence. To cover typical supra-thermal electron precipitating fluxes, the sensor will need to be capable of measuring differential energy

25 fluxes of 10^6-5x10^9 eV/[cm^2 s sr eV] with good statistics in this 10s interval, without saturating.

ENA instrument will measure neutral atoms in the range from ~5keV to ~200keV, which covers the typical range of significant energy density in ENAs generated by charge exchange in the ring current. In common designs, instruments use a thin-window, low-threshold, pixelated solid-state detector (SSD) to measure precipitating ENAs, and the SSD is read out with a low-resource ASIC. Counts can be flexibly accumulated on an instrument FPGA to match the science requirements.

30 Electrostatic deflection will need to be used to sweep low energy charged particles out of the instrument field of view. The pixelated SSD will allow for coarse imaging of the ENA flux as well as refined separation of ENAs from energetic charged particles.

4.2.5 Ion Mass Spectrometer (IMS) and Neutral Mass Spectrometer (NMS)

The IMS and NMS instruments will measure the composition and density of the main ion and neutral species along the spacecraft orbit; more specifically of ion species H^+, He^+, N^+, O^+, NO^+, O_2^+ and of neutral species H, He, N, O, N_2, NO, O_2 (and desirably CO_2) in the altitude range ~100 km to >500km. The threshold mass resolution M/dM is ~30, driven by the

5   requirement to separate between NO and O_2. The target mass range is driven by the heaviest species; a mass range of ~>40 is adequate to resolve up to Argon with margin. It is noted here that the spacecraft propellant will need to be selected so as not to interfere with NMS measurements. Regarding the dynamic ranges, as it can be seen from **Fig. 5** the altitude ranges from 100 to 500 km correspond to density variations from ~10^2 to 10^6 /cm^3 for the ions and from ~10^4 to 10^{14} /cm^3 for the neutrals and to temperature variations from 200 to 2000 K. Furthermore cross-track and along-track ion drift and neutral wind

10   velocities can vary in the range of ± -4 km/sec and ± 1 km/sec respectively. Because of the relatively cold temperatures the thermal velocities $\sqrt{(KT/m_{in})}$ of the various particle species (e.g. 1.8-5.7 km/sec for H, 0.9-2.86 km/sec for O, 0.64-2 km/sec for O_2) are significantly smaller than the spacecraft velocity of ~8 km/sec and on the same order of magnitude as the ion drift and neutral wind speeds. As a result the various ion and neutral particle velocity distributions will appear like beams (i.e., wider for high temperature light species and narrower for low temperature heavy species) on the spacecraft frame of

15   reference. The bulk peak energies vary proportionally to V^2 with V in the range 4-12 km/sec for ions and 7-9 km/sec for neutrals (0.08-0.75 eV for H^+, 0.26-0.42 eV for H, 2.5-24 eV for O_2^+, 8.3-13.5 eV for O_2); the bulk beam angle with respect to the spacecraft ram vector vary in the range ±26.5^o for ions and ±7.1^o for neutrals. To adequately capture the distributions the IMS and INS should be designed with a FoV of ±75° for ions and ±21° for the neutrals and for energy range up to 0-35 eV. Therefore the particle flux measurements of each species on the spacecraft frame of reference as a function of the look

20   direction in polar coordinates (θ, φ), can be written as $R_{sc\_in}(\theta, \varphi)$ = F(A, N_{in}, T_{in}, E_{in}, V_{in}, V_{sc}, Alt_{sc}), where A is the instrument aperture area, N_{in}, T_{in}, E_{in} are the density, temperature and energy for each ion/neutral species, and V_{in}, V_{sc}, Alt_{sc} are the vectors for the ion drift / neutral wind velocities, the spacecraft velocity and spacecraft attitude. Because of the frequent collisions at low altitudes the particle distributions for each species can be well approximated as Maxwellian distributions (in the general case with kappa distributions) drifted at the vector sum velocity of $V_{in} + V_{sc}$. With a multi – parameter fit of the

25   flux measurements $R_{sc\_in}(\theta, \varphi)$ and minimizing the least mean square error one can get the total solution for the density of the various ion and neutral densities N_{in}, temperatures, and of the ion drifts and neutral winds. Because of redundancy, the proposed IMS/INS suit will emphasize in the mass analysis and sampling of the relative densities of each species, taking inputs the ion/neutral temperatures and drift/wind vector measurements from the dedicated IDM/RPA and CWS/RWS instruments.

30   The proposed mass spectrometer method is based on electronically gated Time of Flight (ToF), in which an acceleration voltage of few hundred volts energizes up all particles to about the same energy and orders the velocity of all the ions according to the square root of their mass. An electric gate controls the flow of particles from the gate to the detector. The mass of the particles is determined from the ToF measurement at the particle energy. Unlike usual plasma mass analysers

based on foils, the gated ToF method is non-destructive and therefore well suited for molecular species. Contrary to other methods that scan the mass spectrum (quadrupole mass spectrometers), the ToF method measures all particles simultaneously, a key capability for fast sampling in the transition regions. Also most importantly the electronic gating allows controlling the geometric factor and boosting the detector bandwidth by several orders of magnitude beyond the

5   continuous detector capability of $\sim 10^7$ cps. This feature enables handling the neutral density dynamic range of $\sim 10^{10}$ and the sampling requirement of >=16 samples per second. Heritage of gated ToF IMS and NMS include instruments flown onboard the Exocube mission (launched in January 2015 in high inclination LEO orbit) and the Dellingr mission deployed in November 2017 from the ISS (Paschalidis et al., 2016; Paschalidis et al., 2019).

In a common design, the core sensor consists of a top-hat electrostatic analyser, surrounded outwards by a circular gate, by

10   an RPA, by a collimator and by deflectors; thus the sensor can intrinsically cover the entire 4pi sky with the deflector scanning. However for the main satellite the FoV will be limited to +/-90° azimuth and +/-75° elevation scanning and the IMS will be performing mass analysis for each look direction. Although the angular imaging will be redundant to the IDM, it can be useful in areas of low densities where IDMs are limited in sensitivity. In addition, although the RPA feature of the IMS will be redundant to the dedicated RPA instrument, the IMS/RPA can be used to block low energies and to do mass

15   analysis on the non-thermal tail of the ion distributions. Without the elevation and RPA scanning the IMS performs mass analysis in each azimuth direction. Thus the IMS will do faster relative density sampling of each species and the dedicated IDM/RPA instruments could be used for calibrating for total density, temperature and in-track and cross-track ion drifts.

It should also be noted that the best orientation of the IMS and NMS instruments will be with the long FoV (azimuth) on the horizontal plane and perpendicular to the ram direction, in order to match the larger horizontal ion drift and neutral winds

20   compared to vertical. This orientation will reduce or eliminate the vertical scanning (elevation) and thus simplify the instrument design.

4.2.6 Electric Field Instrument (EFI)

The Daedalus Electric Field Instrument (EFI) will be designed to make high-accuracy measurements of in-situ electric fields, spacecraft surface potential and plasma density. The arrangement of six spherical probes mounted near the tips of six

25   deployable stacer booms will enable 3D in-situ measurements using the well-established double probe technique (e.g. Mozer, 2016). Boom orientation will be such as to minimize interference due to the spacecraft plasma wake (e.g. Cully et al., 2007), as in **Fig. 11**, and to minimize optical shadowing of probe surfaces by the spacecraft body and its protrusions. Each probe will also measure electric potential relative to the s/c. The probes will be current-biased to ensure steady plasma sheath resistance, and therefore steady instrument gain at low frequencies (Bale et al., 2008). In the Daedalus plasma

30   environment (120 km to 500 km), rigid booms of lengths > ~4m place the probes many Debye lengths from the s/c, minimizing errors due to s/c surface potential inhomogeneity. A voltage-biased 'stub' element will mechanically support each probe and provide electrical isolation from the booms. Each probe will contain a low-noise, high impedance preamplifier, able to pass signals to the s/c. With 8.2 m probe separation, electric fields up to ~3.6 V/m can be measured.

This range is sufficient to measure geophysical electric field variations on top of the electric field induced by spacecraft motion (up to ~450 mV/m near perigee). The high oxygen density in Daedalus' orbital environment, in particular near perigee, will cause EFI probe surfaces to oxidize. Oxidation of probe surfaces can create an electrically resistive layer on the probe surface (Ergun et al. 2015), or it can erode probe coatings entirely (Vistine 1983, Vistine et al. 1985). Either effect can

5   degrade or destroy the ability of EFI to measure DC-coupled electric fields (Mozer et al. 2016). EFI probes coatings will need to be selected so as to mitigate the effects of oxidation to maintain instrument performance. In the double-probe technique, signals from the probes are passed to the EFI electronics box (EB), where they undergo analog processing, including amplification and filtering. The EB will also contain components for driving probe and stub biases and possibly electronics to support a relaxation sounder. All science signals will be digitized by analog-to-digital converters (ADCs) and

10   will undergo digital processing. Digital algorithms will produce time-series waveform and spectral data products with a wide range of selectable cadences. The EFI may also include a relaxation sounder to measure the local plasma density with high accuracy (Trotignon et al. 2003, Andersson et al. 2015). Alternatively a Mutual Impedance Probe (MIP) or a Langmuir Probe (LP) will be considered, both of which are capable of measuring the local plasma density as well as temperature.

The EFI design as proposed to ESA has the following heritage: Preamplifier designs for EFI instruments have strong

15   heritage. The proposed stacer booms have direct heritage from the French DEMETER mission (Parrot et al. 2002). The preamplifier design has strong heritage from MMS/FIELDS/ADP (Ergun et al. 2016), while the EFI signal-processing heritage includes THEMIS/EFI (Cully et al., 2008), Van Allen Probes/EFW (Wygant et al., 2013), MAVEN/LPW (Andersson et al., 2015), MMS/FIELDS (Ergun et al., 2016), and Parker Solar Probe/FIELDS (Malaspina et al., 2016). The relaxation sounder has direct heritage to MAVEN/LPW (Andersson et al., 2015), whereas the MIP would inherit from the

20   Rosetta/RPC (Trotignon et al, 2007). In each case antenna geometry and frequency range should be adapted appropriately for the Earth's ionosphere. Other heritage electric field instruments include those flown onto ISEE3 (Scarf et al., 1978), and Cluster. In each case antenna geometry and frequency range will be adapted appropriately for the Earth's ionosphere.

4.2.7 Magnetometer (MAG)

High-precision measurements of in-situ magnetic fields are crucial for Joule heating estimates, for deriving current structures

25   in the ionosphere and for studying and interpreting EPP fluxes and magnetosphere-ionosphere current systems. The Daedalus magnetometers will measure both DC and AC magnetic fields: DC magnetic field measurements are a required measurement in **Eq. (1)** and **(4)** of Joule heating and **Eq. (5)** of Pedersen conductivity; they are also needed for determining the pitch angles of precipitating charged particles, as measured by the EPDS. DC magnetic field measurements also allow for a quantitative determination of the upward and downward currents traversed by the instrument: there are well-established

30   methods for extracting current measurements from in situ magnetometer data (Ganushkina et al., 2015; Ritter, et al., 2013), but they all rely on a priori assumptions about the structure of the currents. This is because single point magnetometer measurements do not uniquely determine a current structure, as there are typically many current structures that can produce a given magnetometer signature. For this reason it is useful to simultaneously measure particles (electrons and ions), which

provide much-needed constraints on the current estimates. In addition, more accurate determination of the current structures will be enabled during the times of the sub-satellite releases via multi-point measurements. The AC magnetometer measurements are useful for measuring wave phenomena, as electromagnetic waves (such as Alfvén waves) have magnetic signatures that can be detected.

5   Heritage high-precision magnetometers include, e.g., the vector field magnetometer developed by DTU Space, National Space Institute of Denmark, a fluxgate magnetometer developed by the Institut für Geophysik und extraterrestrische Physik of the Technische Universität Braunschweig (Auster et al., 2007, 2008, 2010), a scalar magnetometer developed by the Space Research Institute of the Austrian Academy of Sciences and the Institute of Experimental Physics of the Graz University of Technology, an absolute scalar magnetometers developed by the National Centre for Space Studies and French

10   Atomic Energy and Alternative Energies Commission/Electronics and Information Technology Laboratory (Léger et al. 2015; Fratter et al., 2016). All these magnetometers have been used or are currently deployed in different satellite missions and will ensure the 50 Hz or higher measurement frequency of the magnetic field with the accuracy and cleanness less than 2 nT and 0.1 nT respectively. To achieve these parameters the magnetometers have to be deployed on a boom, such as shown in the aft of the spacecraft in **Fig. 16**, with a length between 0.5 and 2 m; simulations are necessary to determine the exact

15   length, through a trade off between the stability of the satellite and the accuracy of the measurements. In order to perform multipoint magnetic field measurements that will significantly increase the scientific gain, it is recommended to have at least a scalar magnetometer on the sub-satellites.

4.2.8 Global Navigation Satellite System Receiver (GNSS)

Global Navigation Satellite System (GNSS) receivers are commonly used for ionospheric tomography and for Total Electron

20   Content (TEC) measurements. The underlying principle in this technique is that the ionosphere, being a weakly ionized plasma or gas, affects the propagation of GNSS radio signals. In order to quantify the propagation effects on a radio wave travelling through the ionosphere the refractive index of the ionosphere must be specified (Yizengaw and Essex, 1999). The refractive index of the ionosphere, n, is given by the *Appleton and Hartree* equation as: $n = 1 - X/2 = 1 - 40.3\,N/f^2$, where N is the electron density. This expression has been proven to be accurate to better than 1%. Subsequently, knowing the

25   refractive index of the ionosphere, it is possible to derive the total number of electrons in the ionosphere, the parameter of the ionosphere that produces most of the changes on the GNSS signal along the GNSS signal trajectory from each satellite to the observer. TEC is expressed as the number of electrons in a vertical column having a one square meter cross section, and extending all the way from the GNSS satellite to the receiver. Regarding GNSS-derived TEC products, Daedalus will build on the heritage from CHAMP, GRACE and COSMIC. The GNSS receiver will also be used for attitude knowledge.

30   **4.2.9 Sub-satellite Instrumentation**

The proposed Daedalus mission concept includes expendable small sub-satellites in the form of CubeSats that are released from the main satellite. The sub-satellites are released during the main satellite's perigee descent to lower altitudes and, after

the main satellite ascends to higher perigee, the sub-satellite measurements at lower altitudes provide estimates of the vertical gradients and the temporal evolution of key LTI parameters. Different instrument combinations will be investigated. Potential instrumentation and their measurement objectives are discussed below; these will be further investigated during the initial phases of the Daedalus mission defintion: **(a)** Accelerometer and Laser retroreflectors (a light-weight, passive

5 instrument designed to reflect laser pulses back to their point of origin on Earth) can be employed to determine atmospheric density. This will allow resolving the time constant for density increases at lower altitudes after a solar storm and the vertical extent of the density changes due to Joule heating. The sub-satellites that carry accelerometers will need to be 3-axis stabilized. **(b)** Miniaturized INMS can provide composition measurements of the primary constituents at lower altitudes; this will allow resolving the altitude profile of key constituents, while being able to cross-calibrate the INMS on the main

10 satellite and the sub-satellite. In addition, ion and neutral composition will enable estimates of Pedersen conductivity, σ_P at a second point along a field line below the main spacecraft, something never available before via in-situ measurements. **(c)** Miniaturized Energetic Particle instruments, to determine EPP at lower altitudes and provide the altitude distribution of particle precipitation. **(d)** There have been recent efforts to combine the IDM and RPA instrument functionality into one lightweight, small, low-power unit ideal for small satellites, including CubeSats (*Hatch, 2016; Swenson, 2017*); testing has

15 shown that the design, while saving on power and space, does not compromise much in terms of instrument accuracy relative to using two separate instruments. The combination of an RPA/IDM on the main satellite and on a second point down below would allow the determination of the altitude distribution of ion drifts. Another example includes the Advanced Ionospheric Probe (AIP), with flight heritage onboard FORMOSAT-5 satellite (*Lin et al., 2017*); the AIP is an all-in-one plasma sensor that measures ionospheric plasma concentrations, velocities, and temperatures. **(f)** Magnetometer measurements at a second

20 point below the main Daedalus spacecraft, and at the same orbital plane, will enable observations of currents along similar field lines (with some phase difference, due to the slightly different orbital periods), allowing speculations about the current density gradients as a function of altitude, something that has not been possible before. **(g)** Finally, the sub-satellites can carry a radio occultation measurement device, sending signals to the mothership. The signals from the radio occultation device will be used to determine the density in the vicinity of the mothership, which makes an in situ measurement.

25 Together, these signals can be used to make a 3D tomography of the density structure for the first time.

4.3 Further Observational and Measurement Requirements Relevant to the Mission Concept

In the following, we provide further details of observational and measurement requirements placed on the Daedalus mission concept in terms of the observation geometry and placement of the instruments, the observing scheme of the main satellite combined with the sub-satellites, spatial and temporal coverage and resolution, and a preliminary assessment of accuracy

30 requirements; these will be further consolidated during the first phases of the Daedalus mission definition.

4.3.1 Observation Geometry

The following key scientific instrumentation needs to be placed in the Daedalus spacecraft ram direction: IDM-RPA (or TII), IMS-NMS, RWS-CTS. Three-axis stabilization is required with stringent attitude control and pointing knowledge requirements. The need to perform in-situ measurements in the Lower Thermosphere - Ionosphere is best realized by a

5   spacecraft with minimal cross-section and with body-mounted solar panels to minimize drag effects. A preliminary design of Daedalus with extended electric field booms and an overview of the instrumentation that needs to be placed in the ram direction of the spacecraft, thus defining the minimum cross-section, are shown in **Fig. 11**.

4.3.2 Observing Scheme

Daedalus will perform the episodic descents to lower altitudes during times of varying solar wind conditions to parameterize

10   the response of the LTI to external driving. Initially the episodic descents will be planned during quiet times, when thermosphere density and satellite drag are lower; subsequent descents will be performed during active times, planned based on space weather predictions. Descents can be performed in a step-wise manner, in order to perform measurements at different perigee altitudes, and also to ensure safe descents and to avoid excessive loss of spacecraft velocity due to unexpectedly high satellite drag. An overview of the observing scheme through the complex high-latitude current system is

15   given in **Fig. 12**. The orbits of the main (green) and a sub-satellite (red) are shown both for the mission phase when perigee is at high latitudes (solid lines), when the satellite can perform in-situ measurements in the region where Joule heating maximizes, and also at times when apogee is at high latitudes – due to precession of the orbit's semi-major axis (dashed lines), when vertical gradients of Field-aligned currents and EPP can be investigated. Schematic locations of the Pedersen, Hall and Field-aligned currents are also drawn. Several mission scenarios can be executed: If a sub-satellite is released in

20   association with a solar storm then one can look at the time history during and after the storm; by quantifying Joule heating in-situ and by monitoring the density enhancements and composition changes at various altitudes below, Daedalus will allow estimates of the extent and distribution of the Joule heating region and enable calculation of the total energy deposition during the storm. When the perigee is at low-latitudes, dynamo mechanisms can be studied with two-point observations, ideally with one point in the E-region and one point in the F-region, such that the actual creation of the dynamo can be

25   observed at low altitudes and the effects of the dynamo mechanism can be observed at high altitudes. Daedalus can also test theoretical explanations for the equatorial anomaly (*Appleton, 1946*), which has not been measured in-situ before with multi-point measurements.

4.3.3 Spatial Coverage and Spatial Resolution

The region of interest for the primary science objectives is from 100 to 200 km, however measurements will be performed

30   from altitudes of 500 km and downwards in order to provide context measurements and to cover the entire range where Joule heating and other energy transport processes take place. The upper limit of 500 km is set due to limitations in the maximum

dynamic range that the IMS and NMS can achieve, but can be extended upwards on a per instrument basis in order to allow conjunctions with other missions at higher circular orbits and/or the investigation of phenomena that extent to higher altitudes. Instruments such as EFI, MAG and EPDS can operate along the entire orbit, to allow additional science objectives to be addressed. An example of the relation between spatial resolution and temporal resolution is given in **Fig. 13**, obtained

5   through sampling the NRLMSISE-00 model along the simulated orbit.

It should be noted that vertical resolution is a very important parameter, more critical than horizontal resolution, as, to first order, the vertical profile determines to a larger degree how energy is distributed, rather than the longitudinal profile. A secondary consideration is the latitudinal structure of the observed features. An initial vertical resolution of 0.5 km for the in-situ sampling of key LTI parameters is baselined, with a higher threshold resolution of 0.25 km at altitudes below 150 km,

10   during the perigee descents. Regarding the latitude-longitude coverage, it is preferable to keep perigee at as high a latitude as possible, which is a trade-off in the ellipticity of the orbit: the more elliptical the orbit, the less the perigee precesses. However the more elliptical the orbit, the longer the orbital period becomes and thus the revisit time at perigee suffers. Finally, perigee precession allows measurements at both at high and low latitudes to be performed, thus allowing measurements of Joule heating and EPP at high latitudes and also the equatorial electrojets. These will be determined

15   through a trade-off analysis; an example of the long term evolution of Daedalus argument of perigee, inclination, right ascension of the ascending node and eccentricity for the sample orbit of **Fig. 10** are shown below in **Fig. 14**.

4.3.4 Temporal Coverage and Temporal Resolution

The temporal coverage needs to be reconcilable with the spatial and temporal scales of the phenomena under investigation. In general, the thermosphere and ionosphere have a response and relaxation time on the order of days. At low latitudes the

20   dynamics are a diurnal phenomenon, but one that can change every day. The measurement strategy of Daedalus will be to measure all local times with a precessing satellite. At mid- and high-latitudes dynamic timescales are on the order of hours: for example, Joule heating happens over the course of several hours. During a large storm, the dynamic timescale is days. This, in turn, defines the timescale required for the repeat cycle. In the mission concept described herein, the main spacecraft has an orbital period of ~120 min and will provide the required temporal coverage to identify diurnal variations and the

25   response and relaxation of the LTI to external solar driving. At the same time, the combination of the main spacecraft with sub-satellites will provide measurements to separate temporal from spatial effects and will also enhance the repeat cycle of the main satellite with context measurements. Regarding temporal resolution, all instrument signals will be recorded below 500 km at ≥16 sample/s, giving a horizontal resolution ≤1 km. Brief segments will be recorded for later playback as 'burst' data, especially during the deep-dips of the spacecraft, or other selected time intervals.

30   It is noted that the sub-satellites will be released at a lower perigee and they will have a different cross-section-over-mass ratio than the main satellite as well as different drag coefficients; thus they will be flying at slightly different velocities than the main satellite. This means that measurements at two different altitudes over the same latitude-longitude will have a temporal offset that will increase as the satellites drift apart, as shown in the orbital simulations of **Fig. 15**. The maximum

temporal offset for the co-registration of measurements by the main satellite and the sub-satellite will be equal to half the orbital period, or ~60 minutes. However the time-scales of events under investigation are on the order of several hours to days; thus the maximum temporal offset between the measurements at the two altitudes is acceptable and provides important information for the spatial/altitude scale of events in the LTI.

5 **4.3.5 Measurement Accuracy Requirements**

To address the primary science objectives of Daedalus, and in particular the determination of Joule heating, precise vector neutral wind and ion drift measurements are required. The most stringent stability and alignment requirements are dictated by the IDM and the neutral wind sensors (RWS and CTS). The IDM needs to be pointing constantly towards the direction of travel of the spacecraft (ram direction). Thus 3-axis stabilization is required. 3-axis stabilization is also ideal for particle
10 measurements. Thus the spacecraft should be aligned so that the first axis always points towards the ram direction (horizontal axis), the second axis points towards the center of the earth (vertical axis) and the third axis completes the orthogonal system (horizontal axis). Instruments for ion drift and neutral wind determination have commonly a FoV of $\pm45^{o}$; this could be aligned in the ram direction, since generally pointing is known better in that direction. A trade-off analysis should be conducted to identify the optimal means to achieve the required alignment; it is noted here that reaction wheels
15 will potentially hinder accelerometer measurements, which are needed for density determination. Errors in pointing knowledge will propagate onto errors in ion and wind speeds; for the Daedalus spacecraft orbit at perigee, 1 degree of error in pointing knowledge corresponds to 140 m/s error in knowledge of ion drifts and winds. Observation requirements for Joule heating determination lead to an estimated required spacecraft pointing knowledge to within 0.02^{o} accuracy in the vertical direction (< 3 m/s accuracy in ion drift & wind speed) and 0.14^{o} accuracy in the horizontal directions (< 20 m/s
20 accuracy in ion drift & wind speed); these will be consolidated during the initial phases of the Daedalus mission definition. To achieve the above pointing knowledge and alignment, 2 star cameras are baselined.

4.4 Spacecraft Design Constraints and Design Considerations

The low altitudes that Daedalus targets pose a number of technical challenges. To overcome these challenges, the original design of Daedalus was based on the following criteria, and an initial layout with subsystems as shown in **Fig. 16**:

25 **4.4.1 Spacecraft Structure**

The structure of the main Daedalus spacecraft should employ an aerodynamic design to compensate for increased drag during perigee passes at low altitudes. The minimum cross-section is determined by the ram direction instrumentation and by the cross-section of the deployed electric field booms. The former should be minimized in collaboration with instrument designers and the latter should be designed as narrow as possible while maintaining stability and rigidity in the high-drag
30 environment during perigee. The preliminary design has a cross-sectional area of 0.4 m^2 for the spacecraft body and a cross section of 0.2 m^2 for the stacer booms; if these could be significantly reduced, further increases in the mission lifetime could

be realized. The use of special fins or structures should be investigated as part of the Daedalus feasibility studies, to increase the aerodynamic stability while minimizing the drag coefficient (C_d) of the main spacecraft.

4.4.2 Spacecraft Stabilization and Attitude & Orbit Control Subsystem (AOCS) considerations

Three-axis stabilization is a measurement requirement for the ram direction instrumentation; two star-trackers are baselined herein. Instrument pointing knowledge and pointing control requirements pose restrictions on the AOCS. The AOCS design should take into account modes of vibration of the electric field and magnetic field booms. In addition, the release of the sub-satellites and the use of propulsion will cause the spacecraft center of mass to move from its initial position; the use of six (two per axis) mass trim mechanisms, driven on a nut rotor with a stepper motor, would allow the center of gravity of the satellite to be re-adjusted after deep-dip manoeuvres and sub-satellite releases.

4.4.3 Propulsion Subsystem Considerations

The propulsion subsystem should be optimized to maximize the number of designed manoeuvres (21 perigee descents are plotted in **Fig. 10**), while maintaining perigee and apogee to extend the mission lifetime. The propellant should not contain constituents that could contaminate IMS and NMS measurements. Hybrid propulsion systems will be investigated, such as have been proposed for the ESCAPE mission (Danduras, 2019, private communication): one will be used for perigee descent and for manoeuvres, which can be low-I_{sp} and relatively low-thrust, and a high-I_{sp} propellant for ascent.

4.4.4 Radiation Environment Considerations

The highly elliptical orbit of the Daedalus mission means that the spacecraft will cross the inner radiation belt during apogee passes. This becomes particularly significant above ~2,250 km. Thus special measures should be taken to utilize radiation-hardened electronics and/or to shield all critical electronics. Both the main spacecraft and the sub-satellites need to be radiation-hardened. A radiation monitor will be part of the Daedalus payload, in order to assist in safeguarding of the spacecraft operations as well as to characterize the radiation environment.

4.4.5 Spacecraft Thermal Design

At perigee, and in particular during the perigee descents, enhanced free molecular heating rates can lead to significant heating of the spacecraft, in particular at the ram direction. Adequate heat shields and an efficient heat dissipation system should be used to mitigate potential overheating of the ram direction instruments. Electric field booms also need to be tested under anticipated thermal and aerodynamic loads (combined) to ensure that they don't buckle or bend.

4.5 Relation to other Missions and Potential Synergies

The Daedalus mission will complement a series of very successful past missions, and will also by synergistic with a number of planned and current missions; these are discussed in the following:

4.5.1 Relation to Past Missions

5   Several missions have performed in-situ measurements in the lower thermosphere-ionosphere, demonstrating the feasibility of Daedalus measurements: **Swarm** is a current ESA EO three-spacecraft constellation mission to study the Earth's magnetic fields and currents flowing in the magnetosphere and ionosphere. Recently, the **e-POP** instrument package on Canada's **Cassiope** satellite was integrated with Swarm as the mission's fourth element. Two of the Swarm satellites fly side-by-side at 460 km and one at 530 km, and Swarm's fourth element, e-POP, flies in an elliptical, polar orbit, with a perigee of 325 km

10   and apogee of 1,500 km; these are significantly higher than the 100-200 km transition region that is targeted by Daedalus. Swarm measurements include magnetic fields, ion density, ion drift velocity, and non-gravitational accelerations like air-drag, winds, Earth albedo and solar radiation pressure, however Swarm does not carry an ion or a neutral mass spectrometer, and it also does not differentiate actual ion drifts from ExB ion drifts, which are crucial for Daedalus' science objectives in the LTI region. The Daedalus mission's measurements will help extend to lower altitudes several scientific objectives of the

15   Swarm constellation mission, such as investigating electric currents in the magnetosphere and ionosphere and quantifying the magnetic forcing of the upper atmosphere. **MAVEN**, an active Mars mission, successfully performs measurements in the Martian thermosphere-ionosphere from a highly elliptical orbit, and the mission scenario also includes deep-dips into the lower thermosphere, providing complete coverage of the Martian upper atmosphere and its interactions with the solar wind. Measurements include ion and neutral composition, energetic particles and electric and magnetic fields, similarly to the

20   Daedalus concept, as well as neutral and ion winds, using the ion and neutral mass spectrometer. **C-NOFS** targeted the effects of ionospheric activity on signals from communication and navigation satellites. Similarly to Daedalus, it performed in-situ measurements of ion and neutral velocities as well as electric fields using 6 booms from an elliptical orbit; however it had an equatorial orbit, and its perigee was 405 km, much higher than the altitude range targeted by Daedalus. C-NOFS also lacked composition measurements. **Cluster** is an ESA mission consisting of four identical spacecraft flying in a tetrahedron-

25   like formation; it was launched in 2000 into an approximately 4×20 R_E polar orbit with an inclination of about 87° and is still operating. One of the four spacecraft, Tango (Cluster 2), made in 2009 the lowest dip into the ionosphere down to about 200 km altitude, performing field and ionospheric plasma measurements. In addition to these more recent missions, the **Atmosphere Explorers (AE)** of the 1970s and the **Dynamics Explorer (DE)** mission of the 1980s also performed in-situ measurements of density, ion drifts, multi-phase (neutral, ion) composition, and temperature structure down to the heart of

30   the transition region (e.g., perigee of ~150 km and deep-dips down to ~130 km by AE-C, and down to 280 km by DE). These spacecraft lacked neutral wind measurements, with the exception of DE, which for the first time measured the vertical motions of the local wind. It is also noted that the dynamic range of some of the key measurements of the AEs, such as mass

spectrometer composition, made the data interpretation difficult at low altitudes. Remote sensing missions of the LTI include **UARS** (e.g., the WINDI instrument looked at winds and temperature at low and mid-latitudes, at 85 to 250 km) and **TIMED** (which obtained O, O_2, N_2, ion density during daytime). These are among the primary sources of information on the LTI, however for many key processes simultaneous measurements of all key geophysical variables are needed.

4.5.2 Synergy with ground-based instruments

An extensive network of ground-based instruments can provide supplementary context measurements in the ionosphere, and be cross-calibrated in-situ by Daedalus. These include existing networks of Ionosondes, Incoherent Scatter Radars, Coherent Scatter Radars, Auroral Imagers, Photometers and Fabry-Perot Interferometers. In particular the state-of-the-art volumetric **EISCAT_3D** radar will be fully operational in 2022, well-timed with a potential launch of Daedalus in 2027/28, if selected. The radar will provide electron density, electron and ion temperature and vector ion drift velocity between 70 and 1000 km within a 3D cone with a diameter of 500 km at an altitude of 150 km (McCrea et al., 2015). Together, Daedalus and EISCAT_3D would provide the "microscope-telescope" approach of combined in-situ and remote sensing measurements, providing a powerful tool for LTI studies.

5 Discussion and Conclusions

5.1 On the Anticipated Impact of the Scientific Advances of Daedalus

The scientific advances anticipated from the mission are directly relevant to a number of societal issues: **[1]** Daedalus will provide critical information of in-situ composition, and in particular CO_2, to help address the response of the upper atmosphere to global warming in the lower atmosphere and its role in energy balance processes. **[2]** Measurements that Daedalus will perform in the LTI are essential for understanding the exosphere and modelling its altitude density profile and its response to space weather events, as all exospheric models use parameters from this region as boundary conditions. **[3]** Furthermore during geomagnetic storms and substorms, currents with increased amplitudes close through the LTI, producing enhanced Joule (ohmic) heating (Palmroth et al., 2005; Aikio et al., 2012) and leading to significant enhancements in neutral density, which in turn results in enhanced satellite drag. Daedalus will provide critical measurements for Joule heating estimates that can be used as anchor-points in global circulation models. **[4]** Space weather effects enhance ionospheric scintillation of the Global Navigation Satellite System (GNSS) signals, which severely degrades positional accuracy and affects performance of radio communications and navigation systems (Xiong et al., 2016); Daedalus will measure in-situ plasma parameters that are involved in GNSS signal scintillation. **[5]** Sudden enhancements in the current system that closes within the LTI induce GICs on the ground, the impact of which on power transformers in electrical power systems has, in occasions, been catastrophic (Pulkkinen et al., 2017) and is considered a threat to technology-based societies, should an extreme solar event occur. Daedalus will measure in-situ the currents that produce GICs, and will thus assist in the accurate modelling of GICs in response to geomagnetic activity. **[6]** Energetic proton and electron precipitation has a role in

mesospheric ozone destruction, large enough to be important at the atmospheric and climate level (Andersson et al., 2014). So far it has been difficult to assess the impact of the role due to insufficient energy spectrum associated with the precipitation. Daedalus will provide the necessary EPP energy spectrum, together with local composition, to directly assess the role of EPP in upper atmosphere chemistry.

5   Despite its significance to the above societal issues, the LTI region is the least measured and least understood of all atmospheric regions. The continuous and ever-increasing presence of mankind in space and the importance of the behaviour of this region to multiple issues related to aerospace technology, such as orbital calculations, vehicle re-entry, space debris lifetime etc., together with its importance in global energy balance processes and in the production of GICs and GNSS scintillations make its extensive study a pressing need. Daedalus responds to the above societal challenges by providing

10   ground-breaking measurements in a region that has been vastly under-sampled, via innovative orbital manoeuvres and sub-satellite deployments. These observations should be sustained so as to resolve the seasonal variability of key LTI phenomena, as described above, while providing sufficient temporal coverage to resolve the time-scales of dynamic events that lead to upper atmosphere heating. Measurements will be synthesised from a set of individual instruments, each of which provides critical parameters towards the science results. Daedalus will also have synergy with many current and future

15   scientific space missions, such as MEME-X, AWE, TRACERS, GOLD, ICON, GDC and DYNAMIC.

5.2 On the Uniqueness and Complementarity of Daedalus

5.2.1 Uniqueness: Other means for addressing the mission requirements

Some of the required parameters can be measured by ground instrumentation, but Joule heating and EPP cannot be derived accurately based on those measurements, as all required parameters must be measured simultaneously at the same location.

20   In particular, neutral density and wind estimations from the ground are very problematic within the 100-200 km altitude range. Optical methods based on Fabry-Perot interferometers exist for neutral wind, but those require non-cloudy conditions and even then, provide only height-averaged measurements from typically 1 or 2 specific altitudes (e.g. Oyama et al., 2018). In addition, ground stations are inherently limited to a specific location, whereas a spacecraft will eventually cover all local times and latitudes. The uncertainty in obtaining accurate Joule heating estimates between various methods is demonstrated

25   in **Fig. 5**, where different methods vary in their estimates by up to 500% (Palmroth et al., 2005). An in-situ mission with all necessary measurements will provide reference points against which different models and methodologies can be validated and the role of neutral dynamics can be quantified.

5.2.2 Complementarity: Upper Atmosphere activities of other national and international bodies.

On June 28, 2017, NASA has selected nine proposals under its Explorers Program; of these missions, three are directly

30   related to processes in the upper atmosphere, and will complement the science results of Daedalus: **MEME-X** (Mechanisms of Energetic Mass Ejection – eXplorer) will map the universal physical processes of the lower geospace system that control

the mass flux through the upper atmosphere to space potentially transforming our understanding of how ions leave Earth's atmosphere. **AWE** (Atmospheric Waves Experiment) will investigate how atmospheric gravity waves impact the transport of energy and momentum from the lower atmosphere, a fundamental question in Heliophysics. **TRACERS** will study interactions between the solar wind and the magnetosphere from an altitude of 750 km, focusing on cusp electrodynamics.

5 The timeframe for the development of these three missions is well timed with the present EE-10 call and these missions can offer excellent complementarity with the measurements of Daedalus. Two currently active NASA missions are targeting the thermosphere: **GOLD** (Global-scale Observations of the Limb and Disk), operated by NASA, explores the upper atmosphere through full-disk UV images of Earth from geostationary orbit, through which scientists can determine the temperature and relative amounts of different chemical elements present in the neutral gases (O and N_2), which, in turn, help show how the

10 neutral gases shape characteristics of the ionosphere. GOLD was launched on January 25, 2018. **ICON** (Ionospheric Connection Explorer) will study the ionosphere and neutral upper atmosphere in conjunction with GOLD: while GOLD flies in geostationary orbit, ICON will fly 560 km above Earth, where it can gather close-up images of this region. ICON is prepared for launch in 2019. Finally, NASA's next science targets, as outlined in the Heliophysics Decadal Survey, include two reference missions: **GDC** (Geospace Dynamics Constellation), a mission to understand how the atmosphere, ionosphere,

15 and magnetosphere are coupled as a system and to understand how this system regulates the response of all geospace to external energy input; and **DYNAMIC** (Dynamical Neutral Atmosphere-Ionosphere Coupling), a mission targeting the fundamental processes that underlie the transfer of energy and momentum into the Ionosphere-Thermosphere system and to measure the thermospheric and ionospheric variability that lower atmospheric waves cause at higher altitudes.

These missions highlight a new interest for the last exploration barrier, the LTI. However none of these missions plan to
20 study in-situ the key transition region between 100-200 km, where most energy balance processes maximize and where most abrupt variations exist. Daedalus will provide unique and unprecedented measurements in the upper atmosphere to complement and calibrate remote sensing measurements and help develop accurate models of the upper atmosphere. With Daedalus, ESA will assume international leadership in studying the LTI and its processes.

5.2 On the Degree of innovation and the Advancement of EO Capabilities of Daedalus

25 An innovative technology of the Daedalus mission concept is the release on-command of sub-satellites from a mother-ship; this can be used in concepts such as the release on-demand of sub-satellites that can form a constellation for Earth Observation / remote sensing / communications or other applications. Another innovation is the performance of orbital manoeuvres and perigee descents in combination with an efficient propulsion system for orbital maintenance, in order to achieve the lowest perigee achieved up to now by an Earth Observation satellite. Daedalus measurements will help advance

30 upper atmosphere modeling: EPP data along the s/c track will be used to drive ionospheric and thermospheric models such as GLOW (Solomon, 2017) and satellite track models (Emery et al., 1985; Deng et al., 1995; Wu et al., 1996), to calculate the ionization, heating, and composition changes, which can be compared with observations of thermospheric temperatures. These models can use along-track data to derive the global EPP heating. A comparison with observations of thermospheric

temperature can lead to estimates of global Joule heating, based on the differences between EPP model and observations. Daedalus data will be assimilated into TIEGCM and other ionosphere-thermosphere models to provide accurate calculations of global Joule heating and EPP heating. At high latitudes, Daedalus data will be used to build AMIE (Assimilative Mapping of Ionospheric and Electrodynamics) convection maps (Richmond, 1992). Thus, an advancement of EO capabilities is that

5   Daedalus measurements will enable the calibration, assimilation and accurate driving of upper atmosphere models. Daedalus will provide critical information regarding EPP and Joule heating, and it will distinguish between heating sources, something that has not been possible to date.

5.3 Conclusions

The Daedalus mission concept comes at a moment in geophysical sciences when space agencies and international space

10   committees recognize and emphasize the need and the importance of studying the LTI. Understanding the LTI matters in a number of domains, such as orbital calculations, vehicle re-entry, space debris lifetime etc., together with its importance in global energy balance processes and in the production of Geomagnetically Induced Currents (GICs), which are a threat to power transformers and through that to society as a whole. In addition, the LTI acts as a boundary condition to atmospheric models, and its proper characterization is critical for the accurate modeling of a number of processes; with the high level of

15   detail that is required in global climate models, key unknown factors such as the energy balance in the LTI need to be resolved. At the same time, linking magnetospheric electrodynamics models with ionospheric and atmospheric models relies on accurate representation of key processes in the LTI, such as Joule heating, and the correct quantification of key variables, such as conductivities and the particle energy spectrum.

The Daedalus mission concept is also well timed with a number of international space missions that are targeting to measure

20   key properties in the LTI by means of remote sensing; these include the recently selected **MEME-x**, **AWE** and **TRACERS**, the recently launched **GOLD** and the soon-to-be launched **ICON** mission. NASA's decadal survey includes two reference missions that are also targeting ionosphere-thermosphere processes: **GDC** and **DYNAMIC**. Furthermore, the state-of-the-art volumetric **EISCAT_3D** radar (one of the Large-Scale European Research Infrastructures selected by the European Strategy Forum on Research Infrastructures for the next 20-30 years) will be fully operational in 2022, well timed with Daedalus, and

25   will provide time-series of ionospheric parameters over Northern Scandinavia. Daedalus will provide in-situ validation and cross-calibration of these parameters and will also enable extension of these measurements along its orbit. With regard to technical constraints, the Daedalus mission concept builds on a series of very successful missions with features that are similar to those of Daedalus, such as the aerodynamic shape of **GOCE** and its use of propulsion for orbit maintenance, the innovative **Swarm** missions with instrumentation of extreme precision and direct relevance to upper atmosphere scientific

30   issues and the deep-dips of **MAVEN** into the thermosphere of Mars; these missions have successfully demonstrated key technologies for the potential implementation of Daedalus.

References

Ahn, B.H., Akasofu, S.I. and Kamide, Y.: The Joule heat production rate and the particle energy injection rate as a function of the geomagnetic indices AE and AL, J. Geophys. Res., 88, 6275–6287, 1983.

Aikio, A. T., Cai, L. and Nygrén, T.: Statistical distribution of height-integrated energy exchange rates in the ionosphere, J. Geophys. Res., 117, A10325, doi:10.1029/2012JA018078, 2012.

Amm, O., Aksnes, A., Stadsnes, J., Østgaard, N., Vondrak, R. R., Germany, G. A., Lu, G., and Viljanen, A.: Mesoscale ionospheric electrodynamics of omega bands determined from ground-based electrodynamic and satellite optical observations, Ann. Geo- phys., 23, 325–342, 2005.

Anderson, B. J., Takahashi, K., and Toth, B. A.: Sensing global Birkeland currents with Iridium engineering magnetometer data, Geophys. Res. Lett., 27, 4045–4048, 2000.

Andersson, L., Ergun, R. E., Delory, G. T., Eriksson, A., Westfall, J., Reed, H., McCauly, J., Summers, D. and Meyers, D.: The Langmuir Probe and Waves (LPW) Instrument for MAVEN, vol. 195, pp. 173-198, doi:10.1007/s11214-015-0194-3, 2015.

Andersson, M. E., Verronen, P. T., Rodger, C. J., Clilverd, M. A., and Seppälä, A.: Missing driver in the Sun–Earth connection from energetic electron precipitation impacts mesospheric ozone, Nature Comm., doi:10.1038/ncomms6197, 2014.

Appleton, E. V.: Two anomalies in the ionosphere, Nature, 157, 691, 1946.

Auster, H. U., Apathy, I., Berghofer, G., Remizov, a., Roll, R., Fornacon, K. H., Glassmeier, K. H., et al.: ROMAP: Rosetta Magnetometer and Plasma Monitor. Space Science Reviews, 128(1-4), 221-240. doi:10.1007/s11214-006-9033-x, 2007.

Auster, H. U., Glassmeier, K. H., Magnes, W., Aydogar, O., Baumjohann, W., Constantinescu, D., Fischer, D., et al.: The THEMIS Fluxgate Magnetometer. Space Science Reviews, 141(1-4), 235-264. doi:10.1007/s11214-008-9365-9, 2008.

Auster, H. U., Richter, I., Glassmeier, K. H., Berghofer, G., Carr, C. M., & Motschmann, U.: Magnetic field investigations during ROSETTA's 2867 Šteins flyby. Planetary and Space Science, 58(9), 1124-1128 doi:10.1016/j.pss.2010.01.006, 2010.

Bale, S. D., Ullrich, R., Goetz, K., et al.: The Electric Antennas for the STEREO/WAVES Experiment, vol. 136, pp. 529-547, doi:10.1007/s11214-007-9251-x, 2008.

Birkeland, Kristian (1908). The Norwegian Aurora Polaris Expedition 1902-1903. New York and Christiania (now Oslo): H. Aschehoug & Co. out-of-print, full text online at https://archive.org/details/norwegianaurorap01chririch

Burchill, J.K., D.J. Knudsen, B.J.J. Bock, R.F. Pfaff, D.D. Wallis, J.H. Clemmons, S.R. Bounds, H. Stenbaek-Nielsen: Core ion interactions with BB ELF, lower hybrid, and Alfvén waves in the high-latitude topside ionosphere. J. Geophys. Res. 109, A01219, doi:10.1029/2003JA010073, 2004.

Burchill, J.K., D.J. Knudsen, J.H. Clemmons, K. Oksavik, R.F. Pfaff, C.T. Steigies, A.W. Yau, T.K. Yeoman: Thermal ion upflow in the cusp ionosphere and its dependence on soft electron energy flux. J. Geophys. Res. 115, A05206, doi:10.1029/2009JA015006, 2010.

Burchill, J.K., J.H. Clemmons, D.J. Knudsen, M. Larsen, M.J. Nicolls, R.F. Pfaff, D. Rowland, L. Sangalli, High-latitude E region ionosphere-thermosphere coupling: A comparative study using in situ and incoherent scatter radar observations. J. Geophys. Res. 117, A02301, doi:10.1029/2011JA017175, 2012.

Cai, L., Aikio, A. T., and Nygrén, T.: Height-dependent energy exchange rates in the high-latitude E region ionosphere, J. Geophys. Res. Space Physics, 118, doi:10.1002/2013JA019195, 2013.

Carlson, C. W., Curtis, D. W., Paschmann, G., and Michael, W.: An instrument for rapidly measuring plasma distribution functions with high resolution, Adv. Space Res., 2, 67–70, 1983.

Chun, F. K., Knipp, D. J., McHarg, M. G., Lu, G., Emery, B. A., Vennerstrom, S., and Troshichev, O. A.: Polar cap index as a proxy for hemispheric Joule heating, Geophys. Res. Lett., 26, 1101– 1104, 1999.

Codrescu, M. V., Fuller-Rowell, T. J., and Foster, J. C.: On the importance of E-field variability for Joule heating in the high-latitude thermosphere, Geophys. Res. Lett., vol. 22, 17, doi:10.1029/95GL01909, 1995.

Codrescu, M. V., Fuller-Rowell, T. J., Roble, R. G., and Evans, D. S.: Medium energy particle precipitation influences on the mesosphere and lower thermosphere, J. Geophys. Res., 102, 19,977, 1997.

Cully, C. M., Ergun, R. E., and Eriksson, A. I.: Electrostatic structure around spacecraft in tenuous plasmas, Journal of Geophysical Research (Space Physics), vol. 112, pp. A09211, doi:10.1029/2007JA012269, 2007.

Cully, C. M., Ergun, R. E., Stevens, K., Nammari, A. and Westfall, J.: The THEMIS Digital Fields Board, vol. 141, pp. 343-355, doi:10.1007/s11214-008-9417-1, 2008.

Deng, W., Killeen, T. L., Burns, A. G., Johnson, R. M., Emery, B. A., Roble, R. G., Winningham, J. D., and Gary, J. B.: One-dimensional hybrid satellite track model for the Dynamics Explorer 2 (DE 2) satellite, J. Geophys. Res., 100, N A2, 1611-1624, doi:94JA02075, 1995.

Dhadly, M. S., Emmert, J. T., Drob, D. P., Conde, M. G., Doornbos, E., Shepherd, G. G.,... Ridley, A. J.: Seasonal dependence of geomagnetic active-time northern high-latitude upper thermospheric winds, J. Geophys. Res., Space Physics, 123, 739–754. https://doi.org/10.1002/2017JA024715, 2018.

Doss, N., Fazakerley, A. N., Mihaljčić, B., Lahiff, A. D., Wilson, R. J., Kataria, D., Rozum, I., Watson, G., and Bogdanova, Y.: In-flight calibration of the Cluster PEACE sensors, Geosci. Instrum. Method. Data Syst., 3, 59-70, doi:10.5194/gi-3-59-2014, 2014.

Doornbos, E., van den Ijssel, J., Lühr, H., Förster, M., Koppenwallner, G: Neutral Density and Crosswind Determination from Arbitrarily Oriented Multiaxis Accelerometers on Satellites, J. Spacecraft and Rockets, Vol. 47, No. 4, doi:10.2514/1.48114, 2010.

Dunlop, M. W., Balogh, A., Glassmeier, K. H., and Robert, P.: Four-point Cluster application of magnetic field analysis tools: The Curlometer, J. Geophys. Res., 107, 1384–1397, 2002.

Earle, G. D., J. H. Klenzing, P. A Roddy, W. A. Macaulay, M. D. Perdue, and E. L. Patrick: A new satellite-borne neutral wind instrument for thermospheric diagnostics, Rev. Sci. Instrum. 78, 114501 (2007); https://doi.org/10.1063/1.2813343, 2007.

Earle, G. D., R. L. Davidson, R. A. Heelis, W. R. Coley, D. R. Weimer, J. J. Makela, D. J. Fisher, A. J. Gerrard, and J. Meriwether: Low latitude thermospheric responses to magnetic storms, J. Geophys. Res. Space Physics, 118, 3866–3876, doi:10.1002/jgra.50212. 2013.

Emery et al.: Thermospheric and ionospheric structure of the southern hemisphere polar cap on October 21, 1981, as determined from Dynamics Explorer 2 satellite data, J. Geophys. Res., 90, A7, 6553-6566 doi:4A8350, 1985.

Ergun, R. E., Tucker, S., Westfall, J., Goodrich, K. A., Malaspina, D. M., Summers, D., Wallace, J., Karlsson, M., Mack, J., Brennan, N., Pyke, B., Withnell, P., Torbert, R., Macri, J., Rau, D., Dors, I., Needell, J., Lindqvist, P.-A., Olsson, G., Cully, C. M.: The Axial Double Probe and Fields Signal Processing for the MMS Mission, vol. 199, pp. 167-188, doi:10.1007/s11214-014-0115-x, 2016.

ESA's EO Swarm mission: https://earth.esa.int/web/guest/missions/esaoperational-eo-missions/swarm

Fang H., and Cheng, C.: Retarding Potential Analyzer (RPA) for sounding rocket, in: An Introduction to Space Instrumentation, edited by KI Oyama and CZ Cheng, pp. 139–153, 2013.

Fang, X., Randall, C. E., Lummerzheim, D., Wang, W., Lu, G., Solomon, S. C., and Frahm, R. A.: Parameterization of monoenergetic electron impact ionization, Geophys. Res. Lett., 37, L22,106, doi:10.1029/2010GL045406, 2010.

Fok, M. C., et al.: Global ENA IMAGE Simulations. In: Burch J.L. (eds) Magnetospheric Imaging — The Image Prime Mission. Springer, Dordrecht, 2003.

Foster, J. C., St.-Maurice, J.-P., and Abreu, V. J.: Joule heating at high latitudes, J. Geophys. Res., 88, 4885– 4896, 1983.

Fratter, I., Léger, J.-M., Bertrand, F., Jager, T., Hulot, G., Brocco, L., Vigneron, P.: Swarm Absolute Scalar Magnetometers first in-orbit results Acta Astronautica, 121, pp. 76-87. Cited 9 times, doi: 10.1016/j.actaastro.2015.12.025, 2016.

Ganushkina, N. Y., M. W. Liemohn, O. Amariutei, I. A. Daglis, I. Dandouras, S. Dubyagin, D. L. De Zeeuw, Y. Ebihara, R. Ilie, R. Katus, M. Kubyshkina, S. E. Milan, S. Ohtani, N. Ostgaard, J. P. Reistad, P. Tenfjord, F. Toffoletto, and S. Zaharia: Defining and resolving current systems in geospace, Ann. Geophys., doi:10.5194/angeo-33-1369-2015, 2015.

Gary, J. B., R. A. Heelis, W. B. Hanson, and J. A. Slavin: Field aligned Poynting flux observations in the high latitude ionosphere, J. Geophys. Res., 99, 11,417– 11,427, 1994.

Gordiets, B. F., Y. N. Kulikov, M. N. Markov, and M. Y. Marov: Numerical modeling of the thermospheric heat budget, J. Geophys. Res., 87, 4504–4514, doi:10.1029/JA087iA06p04504, 1982.

Hanson, W. B., U. Ponzi, C. Arduini, and M. DiRuscio: A satellite anemometer, J. Astro. Sci., 40, 429, 1992.

Hanson, W., R. Heelis, R. Power, C. Lippincott, D. Zuccaro, B. Holt, L. Harmon, and S. Sanatani: The retarding potential analyzer for dynamics explorer-b, Space Science Instrumentation, vol. 5, pp. 503–510, 1981.

Hatch, W. S.: Plasma velocity vector instruments for small satellites, Master's thesis, Utah State University, Logan, UT, 2016.

Hedin, A. E.: Extension of the MSIS Thermospheric Model into the middle and lower atmosphere, J. Geophys. Res., 96(A2), 1159–1172, doi:10.1029/90JA02125, 1991.

Huba, J. D., R. W. Schunk, and Khazanov: Modeling the Ionosphere-Thermosphere, John Wiley & Sons, vol. 201, 2014.

Kivelson, Margaret G., and Christopher T. Russell: Introduction to Space Physics, Cambridge atmospheric and space science series, Cambridge University Press. ISBN, 0521457149, 9780521457149, 1995.

Knudsen, D. J., J. K. Burchill, K. Berg, T. Cameron, G. A. Enno, C. G., Marcellus, E. P. King, I. Wevers, and R. A. King: A low-energy charged particle distribution imager with a compact sensor for space applications, Rev. Sci. Instrum. , 74, 202–211, doi:10.1063/1.1525869, 2003.

Knudsen, D. J., et al.: Lower-hybrid cavity density depletions as a result of transverse ion acceleration localized on the gyroradius scale, J. Geophys. Res., 109, A04212, doi:10.1029/2003JA010089, 2004.

Kwak, Y.-S., and Richmond, A. D.: An analysis of the momentum forcing in the high-latitude lower thermosphere,

J. Geophys. Res., 112, A01306, doi:10.1029/2006JA011910, 2007.

Laštovička, J.: Trends in the upper atmosphere and ionosphere: Recent progress, J. Geophys. Res. Space Physics, 118, 3924–3935, doi:10.1002/jgra.50341, 2013.

Léger, J.-M., Jager, T., Bertrand, F., Hulot, G., Brocco, L., Vigneron, P., Lalanne, X., (...), Fratter, I.: In-flight performance of the Absolute Scalar Magnetometer vector mode on board the Swarm satellites, Earth, Planets and Space, 67 , doi:10.1186/s40623-015-0231-1, 2015.

Lin, Z. W., C. K. Chao, J. Y. Liu, C. M. Huang, Y. H. Chu, C. L. Su, Y. C. Mao, and Y. S. Chang: Advanced Ionospheric Probe scientific mission onboard FORMOSAT-5 satellite. Terr. Atmos. Ocean. Sci., 28, 99-110, doi: 10.3319/ TAO.2016.09.14.01(EOF5), 2017

MacManus D. H., C. J. Rodger, M. Dalzell, A. W. P. Thomson, M. A. Clilverd, T. Petersen, M. M. Wolf, N. R. Thomson,
5   and T. Divett: Long-term geomagnetically induced current observations in New Zealand: Earth return corrections and geomagnetic field driver, Space Weather, 15, 1020–1038, doi:10.1002/ 2017SW001635, 2017.

Malaspina, D. M., Ergun, R. E., Bolton, M., Kien, M., Summers, D., Stevens, K., Yehle, A., Karlsson, M., Hoxie, V. C., Bale, S. D., Goetz, K.: The Digital Fields Board for the FIELDS instrument suite on the Solar Probe Plus mission: Analog and digital signal processing, Journal of Geophysical Research (Space Physics), vol. 121, pp. 5088-5096,
10   doi:10.1002/2016JA022344, 2016.

McCrea, I., Aikio, A., Alfonsi, L., Belova, E., Buchert, S., Clilverd, M., Engler, N., Gustavsson, B., Heinselman, C., Kero, J., Kosch, M., Lamy, H., Leyser, T., Ogawa, Y., Oksavik, K., Pellinen-Wannberg, A., Pitout, F., Rapp, M., Stanislawska, I., and Vierinen, J.: The science case for the EISCAT_3D radar, Progress in Earth and Planetary Science, 2:21, https://doi.org/10.1186/s40645-015-0051-8, 2015.

15   Mozer, F. S.: DC and low-frequency double probe electric field measurements in space, Journal of Geophysical Research (Space Physics), vol. 121, A10, pp. 10, doi:10.1002/2016JA022952, 2016.

Ogawa, Y., T. Motoba, S. C. Buchert, I. Häggström, and S. Nozawa: Upper atmosphere cooling over the past 33 years, Geophys. Res. Lett., 41, 5629–5635, doi:10.1002/2014GL060591, 2014.

O'Hanlon, J. F.: A User's Guide to Vacuum Technology, 2nd ed., 95, John Wiley, New York, 1989.

20   Olsson, A., P. Janhunen, T. Karlsson, N. Ivchenko, and L. G. Blomberg: Statistics of Joule heating in the auroral zone and polar cap using Astrid-2 satellite Poynting flux, Ann. Geophys., 22: 4133–4142, 2004.

Østgaard, N., Germany, G., Stadsnes, J. and Vondrak, R. R.: Energy analysis of substorms based on remote sensing techniques, solar wind measurements, and geomagnetic indices, J. Geophys. Res., 107 (A9), 1233, doi:10.1029/2001JA002002, 2002.

25   Palmroth, M., Janhunen, P., Pulkkinen, T. I., and Koskinen, H. E. J.: Ionospheric energy input as a function of solar wind parameters: global MHD simulation results, Ann. Geophys., 22, 549–566, 2004.

Palmroth, M., P. Janhunen, T. I. Pulkkinen, A. Aksnes, G. Lu, et al.: Assessment of ionospheric Joule heating by GUMICS-4 MHD simulation, AMIE, and satellite-based statistics: towards a synthesis. Annales Geophysicae, European Geosciences Union, 2005, 23 (6), pp. 2051-2068, 2005.

Palmroth, M., P. Janhunen, G.A. Germany, D. Lummerzheim, K. Liou, D.N. Baker, C. Barth, A.T. Weatherwax, and J. Watermann: Precipitation and total power consumption in the ionosphere: Global MHD simulation results compared with Polar and SNOE observations, Ann. Geophys. 24, pp. 861–872, 2006.

Paschalidis N., S. L. Jones, M. Rodriguez et al.: A Compact Ion Neutral Mass Spectrometer for the ExoCube Mission, 6th
5 European CubeSat Symposium, Estavayet, Switzerland, 2014.

Paschalidis N., S. L. Jones, M. Rodriguez et al. : A compact Ion Neutral Mass Spectrometer for ionospheric measurements – Flight Demo on Exocube and Dellingr missions, under submission, RSI, 2019

Pulkkinen A., E. Bernabeu, A. Thomson, A. Viljanen, R. Pirjola, D. Boteler, J. Eichner, P. J. Cilliers, D. Welling, N. P. Savani, et al.: Vol: 15,; Pages: 828–856; DOI: 10.1002/2016SW001501, 2017.

10 Qian, L., J. Laštovička, R. G. Roble, and S. C. Solomon: Progress in observations and simulations of global change in the upper atmosphere, J. Geophys. Res., 116, A00H03, doi:10.1029/2010JA016317, 2011.

Randall, C. E., V. L. Harvey, C. S. Singleton, S. M. Bailey, P. F. Bernath, M. Codrescu, H. Nakajima, and J. M. Russell III: Energetic particle precipitation effects on the Southern Hemisphere stratosphere in 1992–2005, J. Geophys. Res., 112, D08308, doi:10.1029/2006JD007696, 2007.

15 Richmond, A. D.: Assimilative mapping of ionospheric electrodynamics, Adv. Space Res., Vol 12, No 6, pp (6)69-(6)68, 1992.

Richmond, A. D.: Ionospheric Electrodynamics, in *Handbook of Atmospheric Electrodynamics,* Vol. II (H. Volland, ed.), CRC Press, Boca Raton, Florida, 249-290, 1995.

Rishbeth, H., and R. G. Roble: Cooling of the upper atmosphere by enhanced greenhouse gases—Modelling of
20 thermospheric and ionospheric effects, Planet. Space Sci., 40, pp. 1011–1026, doi:10.1016/0032-0633(92)90141-A, 1992.

Ritter, P., Lühr, H., Rauberg, J.: Determining field-aligned currents with the Swarm constellation mission, Earth Planet Sp 65: 9. https://doi.org/10.5047/eps.2013.09.006, 2013.

Rodger, C. J., Clilverd, M. A., Green, J. C., and Lam, M. M.: Use of POES SEM-2 observations to examine radiation belt dynamics and energetic electron precipitation into the atmosphere, J. Geophys. Res., 115, doi:10.1029/2008JA014023, 2010.

25 Rosenqvist, L., S. Buchert, H. Opgenoorth, A. Vaivads, and G. Lu (2006): Magnetospheric energy budget during huge geomagnetic activity using Cluster and ground-based data, J. Geophys. Res., 111, A10211, doi:10.1029/2006JA011608.

Sangalli, L., D.J. Knudsen, M.F. Larsen, T. Zhan, R.F. Pfaff, D. Rowland, Rocket-based measurements of ion velocity, neutral wind, and electric field in the collisional transition region of the auroral ionosphere. J. Geophys. Res. 114, A4, 2009.

Sarris, T. E., et. al.: Feasibility Study for a Low-Flying Spacecraft for the Exploration of the MLTI Region, Technical Report, ESA/ESTEC, CN 20991, 2010.

Sarris, T. E., et. al.: Electrodynamics Study of the Upper Atmosphere in Support to Future MLTI Missions, Technical Report, ESA/ESTEC, CN 4000104174/11/NL/AF, 2013.

5   Sauvaud, J.-A., Larson, D., Aoustin, C., Curtis, D., Médale, J.-L., Fedorov, A., Rouzaud, J., Luhmann, J., Moreau, T., Schröder, P., Louarn, P., Dandouras, I., and Penou, E.: The IMPACT Solar Wind Electron Analyzer (SWEA), Space Sci. Rev., 136: 227–239, doi: 10.1007/s11214-007-9174-6, 2008.

Scarf, F. L., Fredricks, R. W., Gurnett, D. A., and Smith, E. J.: The ISEE-C Plasma Wave Investigation, IEEE Transaction on Geoscience Electronics, Vol. GE-16, No 3, July 1978.

10 Semeter, J., and F. Kamalabadi: Determination of primary electron spectra from incoherent scatter radar measurements of the auroral E region, Radio Sci., 40, RS2006, doi:10.1029/2004RS003042, 2005.

Seppälä , A., P. T. Verronen, E. Kyrölä , S. Hassinen, L. Backman, A. Hauchecorne, J. L. Bertaux, and D. Fussen: Solar proton events of October–November 2003: Ozone depletion in the Northern hemi- sphere polar winter as seen by GOMOS/Envisat, Geophys. Res. Lett., 31, L19107, doi:10.1029/2004GL021042, 2004.

15 Seppälä, A., C. E. Randall, M. A. Clilverd, E. Rozanov, and C. J. Rodger: Geomagnetic activity and polar surface air temperature variability, J. Geophys. Res., 114, A10312, doi:10.1029/2008JA014029, 2009.

Sinnhuber, M., Nieder, H. & Wieters, N. Surv Geophys: Energetic Particle Precipitation and the Chemistry of the Mesosphere/Lower Thermosphere 33: 1281. https://doi.org/10.1007/s10712-012-9201-3, 2012.

Solomon, S. C., L. Qian, and R. G. Roble: New 3-D simulations of climate change in the thermosphere, J. Geophys. Res.
20 Space Physics, 120, 2183–2193, doi:10.1002/2014JA020886, 2015.

Solomon, S. C.: Global modeling of thermospheric airglow in the far ultraviolet, J. Geophys. Res. Space Physics, 122, 7834–7848, doi:10.1002/ 2017JA024314, 2017.

Sutton, E. K., R. S. Nerem, and J. M. Forbes: Density and Winds in the Thermosphere Deduced from Accelerometer Data, Journal of Spacecraft and Rockets, Vol. 44, No. 6, pp. 1210-1219. https://doi.org/10.2514/1.28641, 2007.

25 Swenson, A. P.: The Field-Programmable Gate Array Design of the Gridded Retarding Ion Distribution Sensor. All Graduate Theses and Dissertations. 6876, https://digitalcommons.usu.edu/etd/6876, 2017.

Thayer, J. P., and J. Semeter: The convergence of magnetospheric energy flux in the polar atmosphere, J. Atmos. Sol. Terr. Phys., 66, 807–824, 2004.

Trotignon, J. G., D'eau, P. M. E., Rauch, J. L., et al.: The Whisper Relaxation Sounder Onboard Cluster: A Powerful Tool for Space Plasma Diagnosis$^{1, 2}$ around the Earth, Cosmic Research, vol. 41, pp. 345-348, 2003.

Trotignon, J.G., Michau, J.L., Lagoutte, D. et al.: RPC-MIP: the Mutual Impedance Probe of the Rosetta Plasma Consortium, Space Sci Rev., 128: 713. https://doi.org/10.1007/s11214-006-9005-1, 2007.

5   Vasyliūnas, V. M., and P. Song: Meaning of ionospheric Joule heating, J. Geophys. Res., 110, A02301, doi:10.1029/2004JA010615, 2005.

Wu, Q., T. L. Killeen, W. Deng, A. G. Burns, J. D. Winningham, N. W. Spencer, R. A. Heelis, and W. B. Hanson: Dynamics Explorer 2 satellite observations and satellite track model calculations in the cusp/cleft region, J. Geophys. Res., 101, N A32, 5329-5342, doi:95JA01819, 1995.

10 Wygant, J. R., Bonnell, J. W., Goetz, et al.: The Electric Field and Waves Instruments on the Radiation Belt Storm Probes Mission, vol. 179, pp. 183-220, doi:10.1007/s11214-013-0013-7, 2013.

Xiong C, Stolle C, Lühr H.: The Swarm satellite loss of GPS signal and its relation to ionospheric plasma irregularities, Space Weather, Vol. 14, pp. 563-577. DOI: 10.1002/2016SW001439, 2016.

Yizengaw, E., & Essex, E. A.: Use of GPS signals to study Total Electron Content of the ionosphere during the geomagnetic
15 storm on 22 September 1999.Victoria: Cooperative research center for satellite systems, 1999.

Yuan, Z., et al.: Influence of precipitating energetic ions caused by EMIC waves on the subauroral ionospheric E region during a geomagnetic storm, J. Geophys. Res. Space Physics,119,8462–8471, doi:10.1002/2014JA020303, 2014

Zhang, X. X., C. Wang, T. Chen, Y. L. Wang, A. Tan, T. S. Wu, G. A. Germany, and W. Wang: Global patterns of Joule heating in the high-latitude ionosphere, J. Geophys. Res., 110, A12208, doi:10.1029/2005JA011222, 2005.

20 Zoennchen, J. H., U. Nass, H. J. Fahr, and J. Goldstein: The response of the H geocorona between 3 and 8 Re to geomagnetic disturbances studied using TWINS stereo Lyman-data, Ann. Geophys., doi:10.5194/angeo-35-171-2017, 2017.

Tables

Source	Energy (W/m²)	Altitude
Solar EUV Radiation	0.003	100 − 500 km
Precipitating Particles		
-- Magnetospheric Protons	0.001 − 0.006	100 − 130 km
-- Magnetospheric Electrons	0.003 − 0.030	70 − 130 km
Joule Heating	0.000014 − 0.140	100 − 500 km
-- E = 1-100 mV/m		
Solar Wind		
-- Kinetic $1/2\rho\upsilon^3$	0.00030	N/A
-- Electromagnetic ExB/μ_0	0.00003	

Table 1: Main energy inputs and ranges in the LTI region.

Instrument	Measurement	Dynamic Range	Accuracy, sensitivity
Ion Drift Meter (**IDM**) & Retarding Potential Analyzer (**RPA**), or Thermal Ion Imager (**TII**)	Ion drifts Ion density Ion Temperature	± 4 km/s [along track and cross track]	100 m/s [along track and cross track]
Ram Wind Sensor (**RWS**) & Cross-track Wind Sensor (**CWS**)	Ram neutral winds Cross-track neutral winds Differential pressure Neutral temperature	± 1 km/s [along track and cross track]	Accuracy ± 10 m/s, sensitivity ± 3 m/s [along track] Accuracy ± 5 m/s, sensitivity ± 2 m/s [cross-track]
Accelerometer (**ACC**)	Neutral density Wind velocity Thrust of propulsion syst.	10^{-7} g to 10^{-3} g	Accuracy $\pm 10\%$ at 500km, $\pm 2\%$ below 200km Sensitivity 10^{-7} g $\pm 3\%$ max systematic error due to uncertainty in drag coefficient
Energetic Particle Detector Suite (**EPDS**), including: • High Energy Instrument (**HEI**) • Low Energy Instrument (**LEI**) • Energetic Neutral Atoms instrument (**ENA**)	HEI: Relativistic Electrons, protons, heavy ions LEI: Low energy electrons ENA: Energetic Neutral Atoms	HEI: 10^1 - 10^6 counts/s LEI: 10^6 - 5×10^9 eV [cm² sr s eV]⁻¹ ENA: energies 5 - 200keV, fluxes 10^2 - 2×10^6 [cm² sr s]⁻¹	HEI: accuracy $\leq 20\%$ LEI: accuracy $\leq 20\%$ for electron energy fluxes above 10^6 eV [cm² sr s eV]⁻¹ ENA: Energy resolution of at least 15 keV, flux to better than 20% for fluxes above 2000 [cm² sr s]⁻¹
Ion Mass Spectrometer (**IMS**) & Neutral Mass Spectrometer (**NMS**)	Ion Composition (IMS) Neutral Composition (NMS) Relative Density	Mass Range: 1-50 amu Ions: H^+, He^+, N^+, O^+, NO^+, O_2^+, CO_2^+ Neutrals: H, He, N, O, N₂, NO, CO₂ Density Dynamic Range: Ions: ~10^2 to 10^6 /cm³ Neutrals: ~10^4 to 10^{14} /cm³ Temperature Range: 200-2000K	Mass resolution accuracy M/dM: ~30 Mass resolution sensitivity: 1 amu Relative density resolution accuracy: 1-10% (TBD) Relative Density resolution: 1%
Electric Field Instrument (**EFI**)	Electric field Preamp Voltage	± 2 V/m ± 16 V (for 8m probe-to-probe separation)	TBD: Requirements will be defined via ionospheric modelling as part of the initial phases of the mission definition
Langmuir Probe (**LP**)	Plasma Density Electron temperature	100-5×10^6 per ccm 200-50,000K (0.02-5eV)	Accuracy $\leq 5\%$ Accuracy $\leq 20\%$ or 200 K
Magnetometer (**MAG**)	Magnetic fields	15000-65000 nT	Accuracy ≤ 2 nT, Sensitivity 10 pT/√Hz at 1 Hz Cleanness ≤ 0.1 nT
GNSS Receiver (**GNSS**)	Total Electron Content	10^{-1}-10^3 TECU	10^{-3} TECU

Table 2: List of Daedalus instruments, measurements, estimated dynamic ranges, accuracies and sensitivities.

Figures
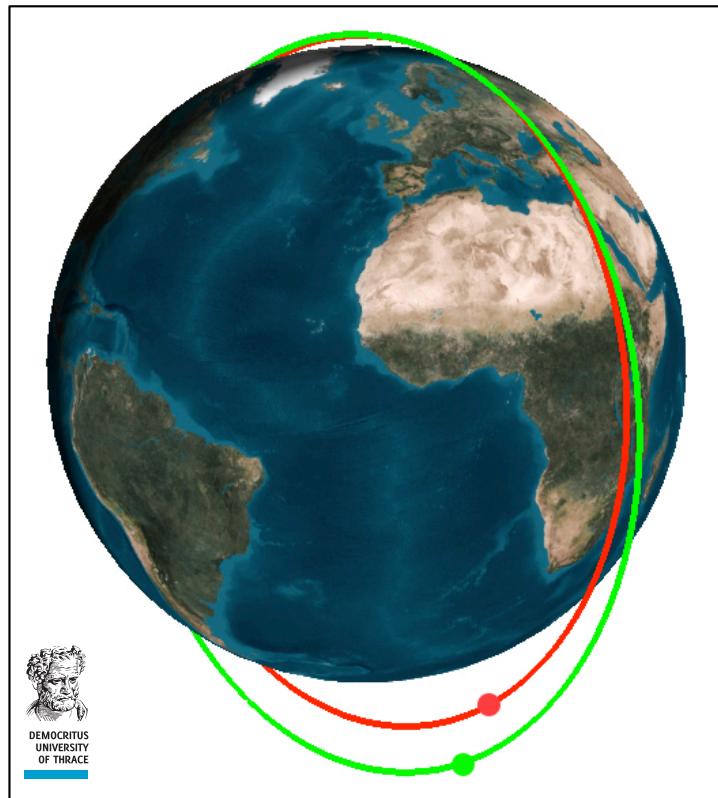
Figure 1: Simulated orbits of the main Daedalus satellite (green) and of a deployed sub-satellite (red).
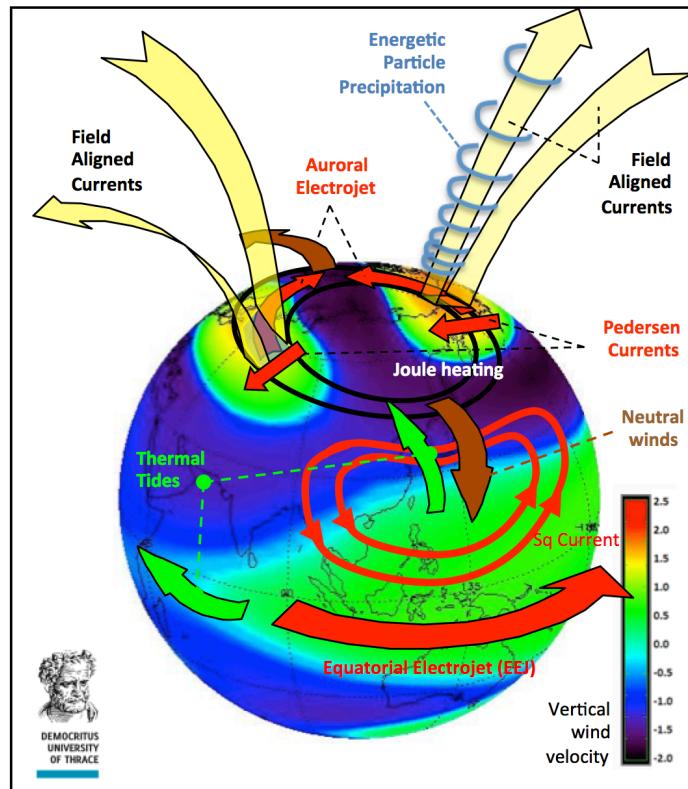
Figure 2: Overview of main processes affecting momentum and energy transport and distribution in the LTI.
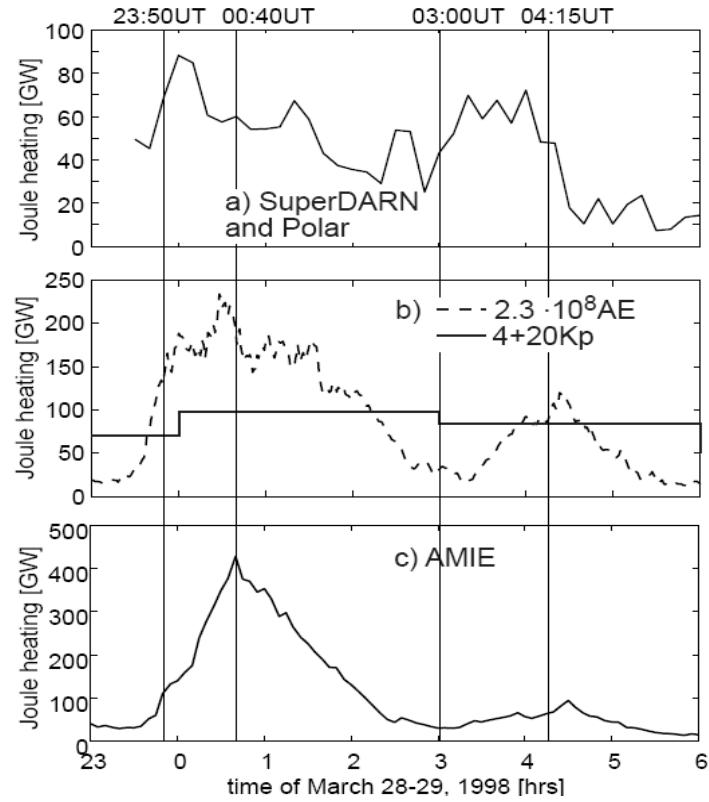
Figure 3: Discrepancies between global integrated Joule heating as estimated by (a) SuperDARN and Polar measurements, (b) AE- and Kp-based proxies, and (c) AMIE procedure during a solar storm (from Palmroth et al., 2005).
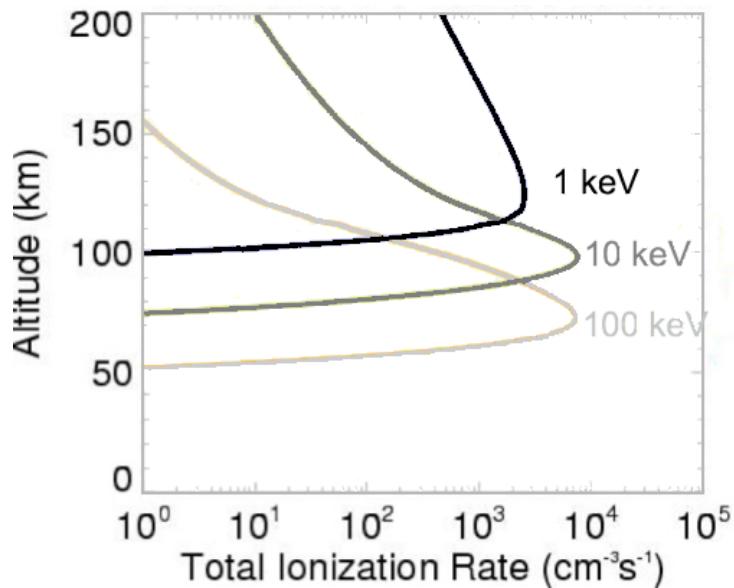
Figure 4: Total Ionization Rates vs. altitude at various energies of precipitating electrons, as marked.
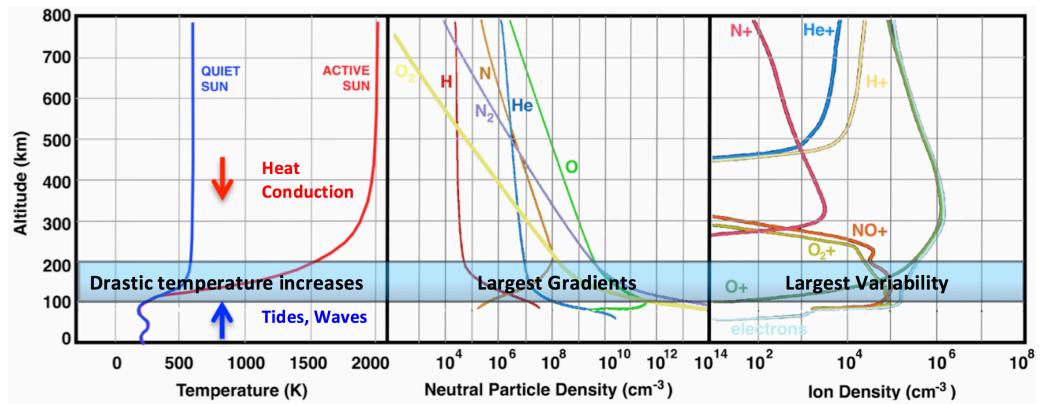
Figure 5: Simulated key variables in the LTI as a function of altitude: Temperature at quiet and active solar conditions (left), neutral (center) and ion (right) constituents. The altitude range from 100 to 200 km shows the largest rates of change in most variables.
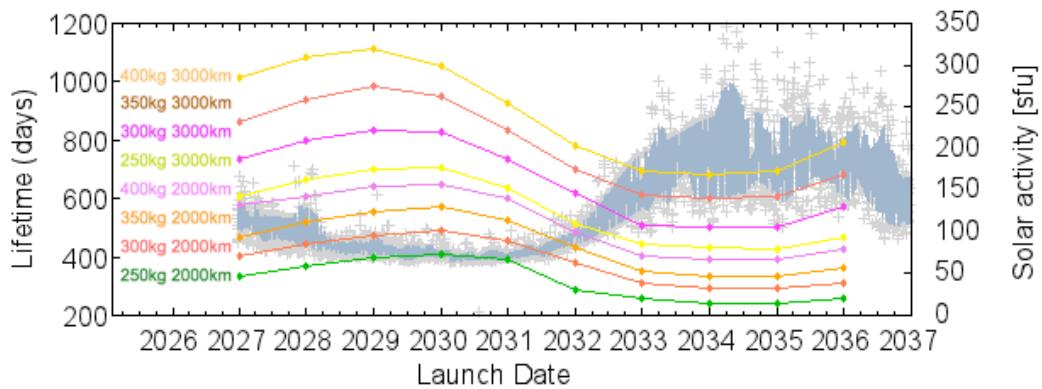
Figure 6: Simulated Daedalus lifetimes as a function of launch date, for a perigee of 150 km and for various values of apogee and spacecraft mass, as marked. It is noted that higher mass and apogee lead to longer lifetimes, whereas higher levels of solar activity lead to shorter lifetimes. Solar activity is plotted in terms of daily (grey crosses) and average (grey lines) values of the F10.7 index.
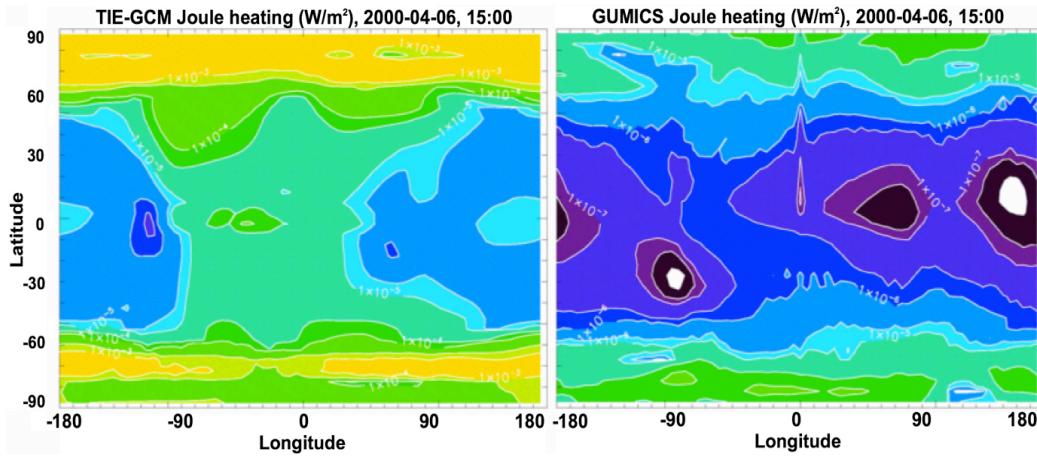
Figure 7: Joule heating from TIE-GCM (left) and GUMICS (right) for the storm of April 6th, 2000 (from Sarris et al., 2013)
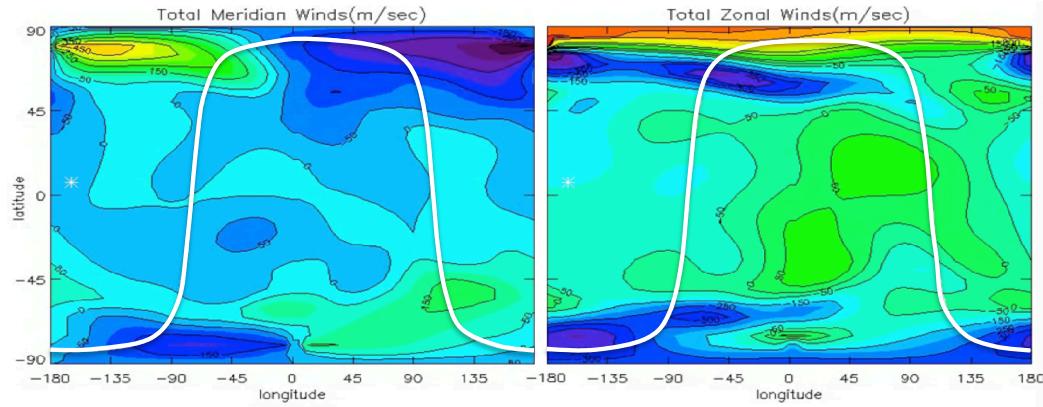
Figure 8: Simulations of Meridional and Zonal winds and ground track of a spacecraft orbit
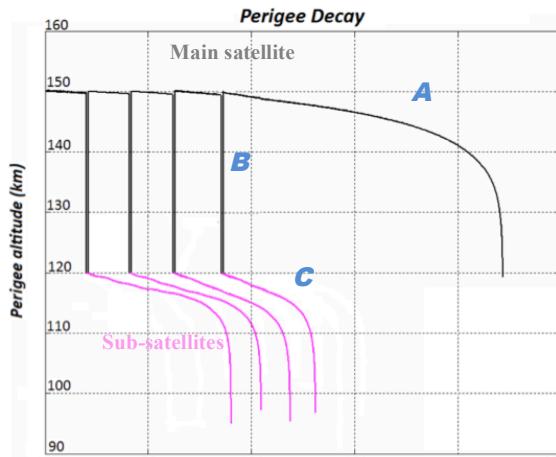
Figure 9: Schematic of the main phases of the perigee history for the Daedalus main satellite (gray lines) and four sub-satellites (magenta lines). The sub-satellites are released during four corresponding descents ("deep-dips") of the main satellite down to 120 km.
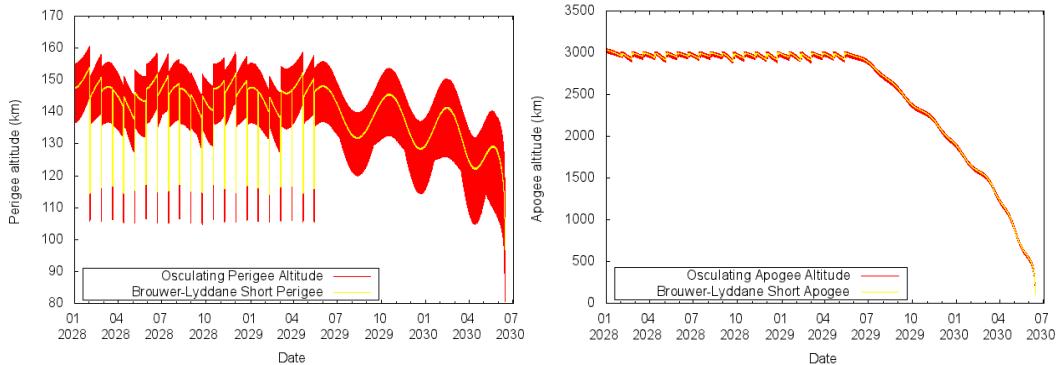
Figure 10: Daedalus perigee (left) and apogee (right) history for a spacecraft launch in 2028, initial apogee at 3000 km and initial satellite mass of 400 kg (including propellant). Apogee and perigee maintenance are employed by means of propulsion.
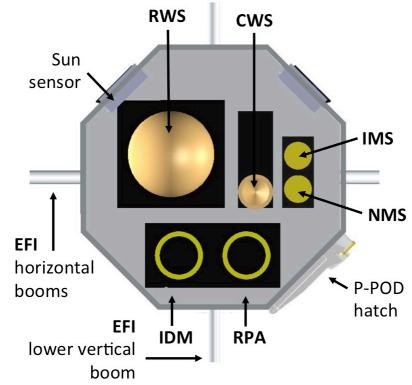
Figure 11: Spacecraft observation geometry: Daedalus s/c with extended field booms; four electric field booms are arranged in X-formation in the along-cross-track plane and two booms are aligned vertically (left). Ram direction instrumentation (right).
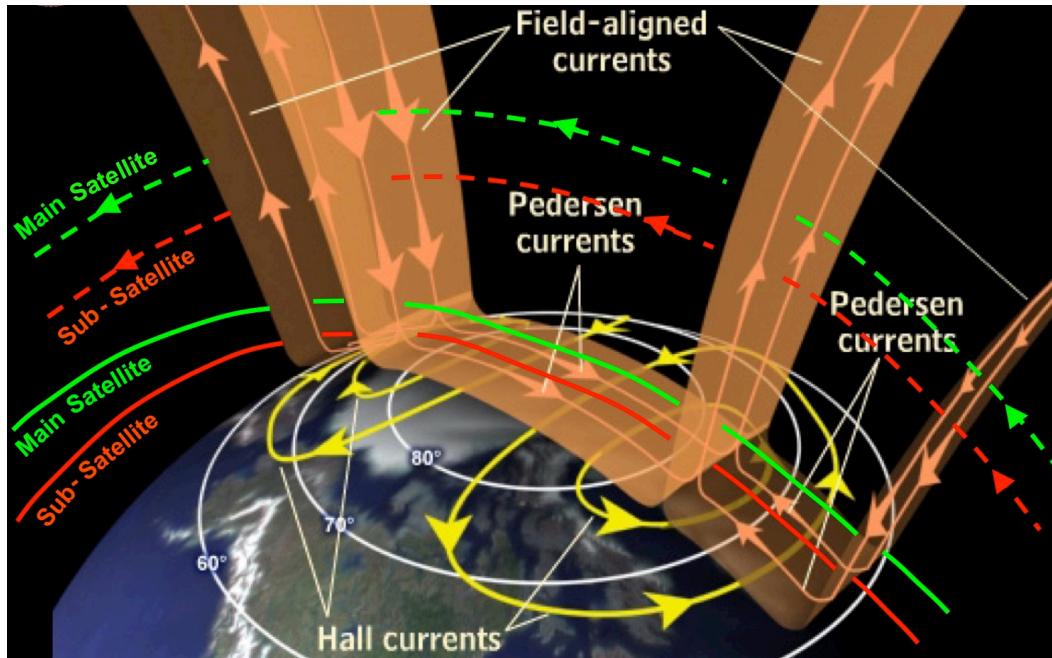
Figure 12: Measurement scheme by the main s/c (green) and a released sub-satellite (red), when apogee is at high latitudes (dashed lines) and when perigee is at high latitudes (solid lines). [adapted from: Gang Lu, The Comet Program, 2007]
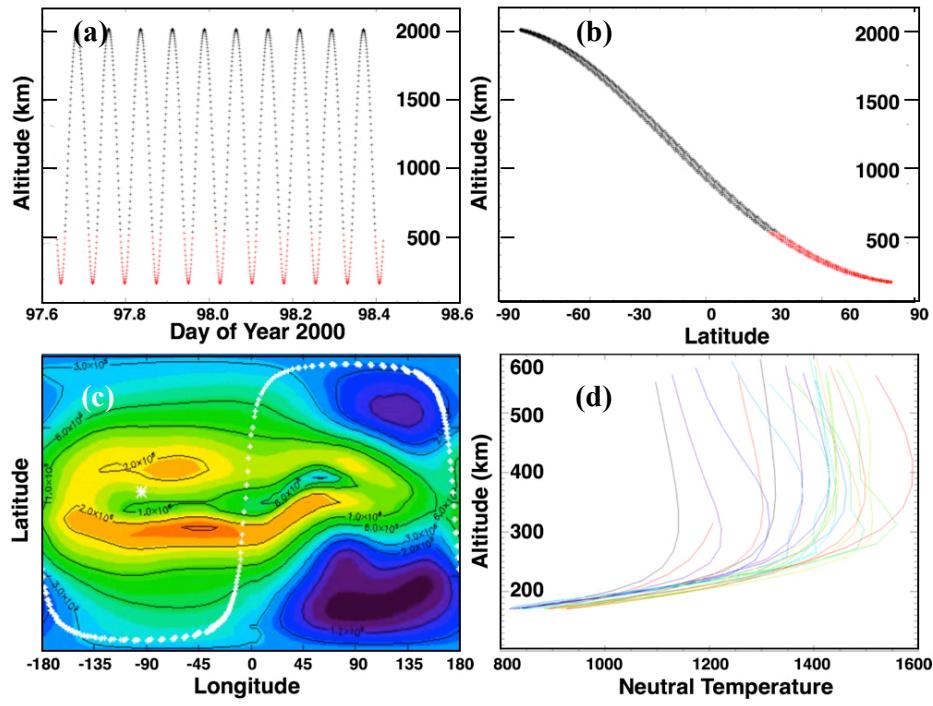
Figure 13: (a) Altitude vs. time for 10 Daedalus orbits; (b) altitude vs. latitude. Red dots: measurements below 500 km. (c) Horizontal sampling (d) vertical sampling of neutral temperature from NRLMSISE along 10 consecutive orbits, during the April 2000 storm.
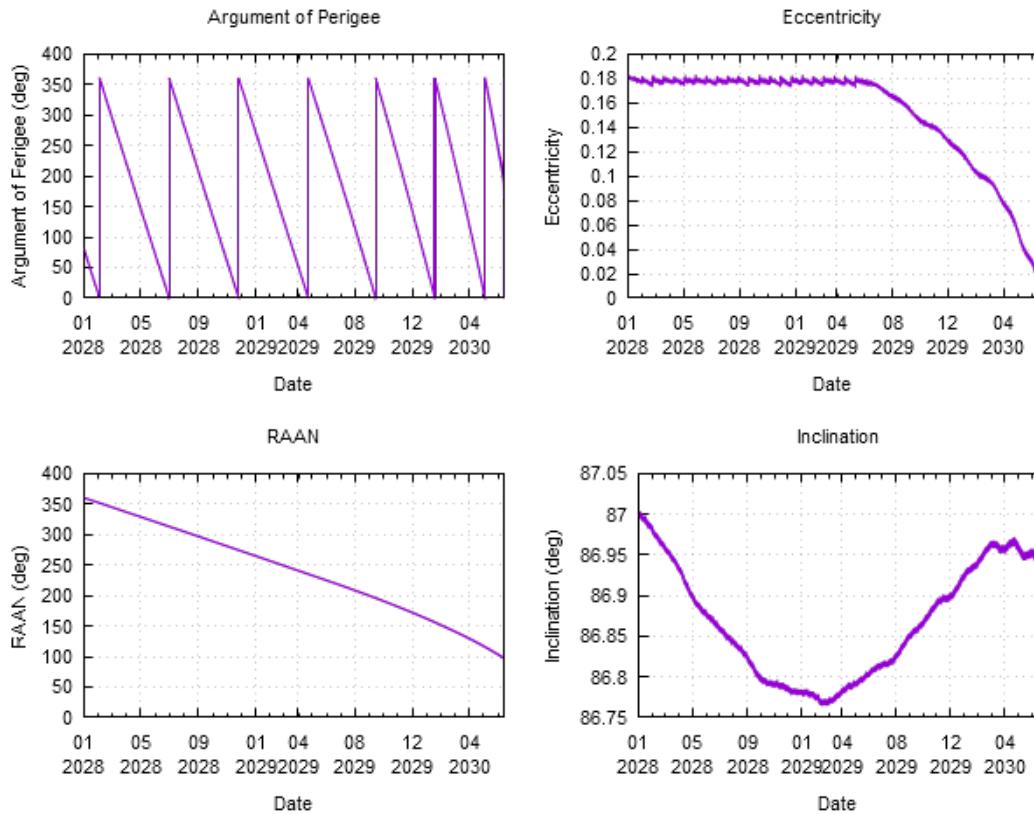
Figure 14: Long term evolution of Daedalus' Argument of Perigee, Inclination, Right Ascension of the Ascending Node and Eccentricity.
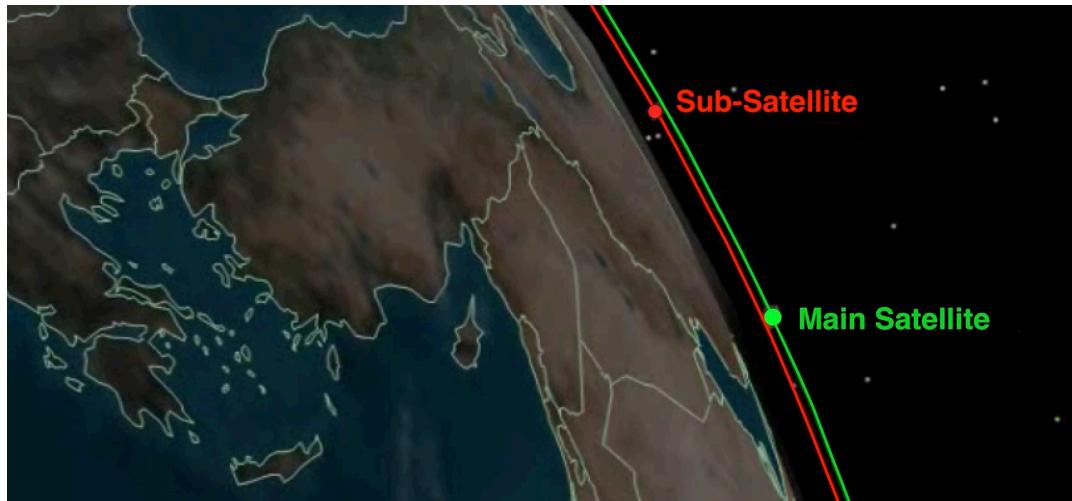
Figure 15: Time offset in the co-registration of measurements over the same location between the main s/c and the sub-satellites
5 **due to different speeds.**
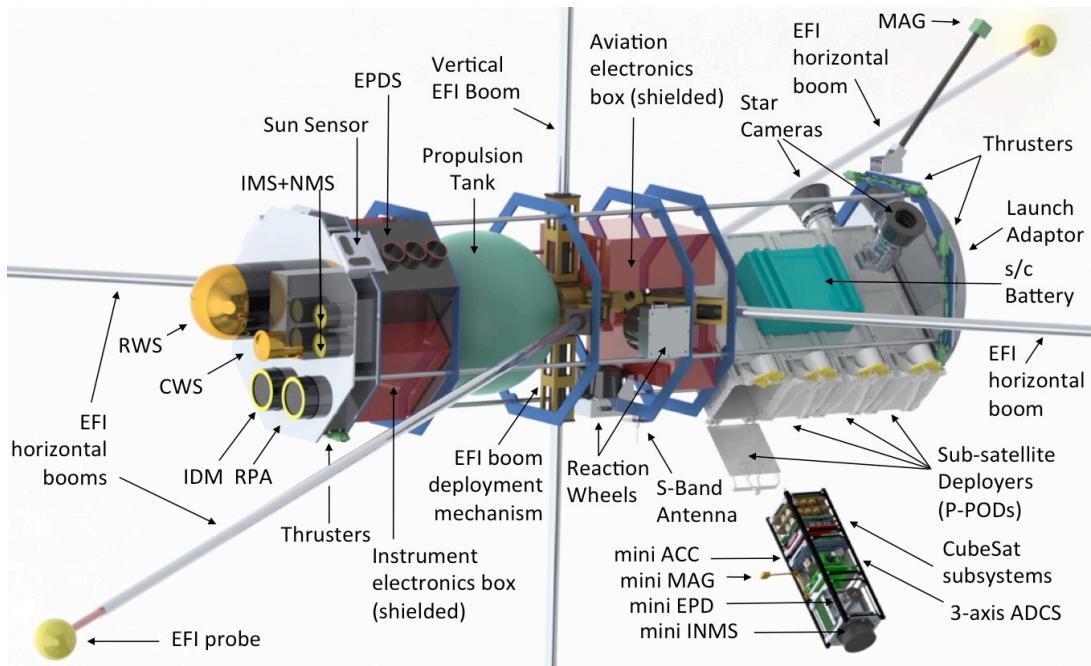
Figure 16: Interior of the main Daedalus satellite, including key s/c subsystems and instrumentation. A deployed CubeSat sub-satellite is also shown, with examples of potential sub-satellite miniaturized instrumentation.